UNIVERSITAT POLITÈCNICA DE CATALUNYA
BARCELONATECH
UPC
Escola Superior d'Enginyeries Industrial,
Aeroespacial i Audiovisual de Terrassa

Design of a swarm of Unmanned Aerial Vehicles for the exploration of Mars

Document:

Report

Author:

Núria Escursell i Serra

Director:

Miquel Sureda Anfres

Degree:

Bachelor in Aerospace Vehicles Engineering

Examination session

Autumn, 2022-23

BACHELOR FINAL THESIS

"Somewhere, something incredible is waiting to be known."

Carl Sagan

Acknowledgements

I would like to express my gratitude to all the people without whom this bachelor's degree thesis wouldn't have been the same.

First of all, I want to thank Miquel Sureda for his support, guidance and help throughout the development of this thesis, for transmitting his passion and enthusiasm, and also to show me the creative side of a field that I love.

Secondly, I want to appreciate my parents without whom I wouldn't have finished this bachelor's degree. Their unconditional support and patience have been essential.

Thirdly, I would like to thank Anna, Lucas and Marc their feedback about this thesis.

Finally, I am greatly appreciated by my friends and family, who have made these four-and-a-half challenging years easier and more pleasant.

Abstract

Mars has been a main target for exploration over the last decades, due to its closeness and similarity to Earth. Exploration landers and rovers have laid the foundation for the understanding of the planet, however, they exhibit some limitations that Unmanned Aerial Vehicles (UAVs) would overcome.

Thus, this report consists of the design of a swarm of UAVs for the exploration of the red planet, which coordinates with a swarm of rovers and a constellation of orbiters that are briefly described.

Firstly, the mission is preliminarily designed to define its location, architecture, objectives, and requirements. Secondly, the single UAV overview is presented, illustrating a preliminary design of all the subsystems involved in order to perform successfully. Thirdly, the swarm of UAVs is defined, introducing pre-flight check procedures. Then, two flight formation algorithms for the swarm of UAVs are suggested, although only one of them is implemented. Fourthly, there is a brief introduction to the multiplatform architecture, focused on communication and connectivity. Finally, conclusions are drawn and and the foundation for future work related to the different chapters of this thesis is included.

Resum

En les últimes dècades, Mart ha estat un dels principals objectius de l'exploració espacial per la seva proximitat i similitud amb la Terra. Diferents mòduls d'exploració espacial i *rovers* han establert les bases per la comprensió del planeta. Tanmateix, presenten diverses limitacions que els vehicles aeris no tripulats (UAVs) poden solucionar.

Així doncs, aquest informe consisteix en el disseny d'una constel·lació de UAVs per l'exploració del planeta vermell, la qual es pretén coordinar amb dues constel·lacions de *rovers* i orbitadors.

En primer lloc, es fa un disseny preliminar de la missió, definint la seva localització, arquitectura, objectius i requeriments. En segon lloc, es presenta una descripció general i individual del UAV, la qual consisteix en el disseny preliminar de tots els subsistemes implicats per assegurar el correcte vol i funcionament del dron. En tercer lloc, es defineix la constel·lació de UAVs, introduint alguns procediments de control previs al vol. A continuació, se suggereixen dos algoritmes de formació de vol per a la constel·lació de UAVs, encara que només s'implementa un d'ells. En quart lloc, s'introdueix breument l'arquitectura general de la missió, la qual se centra en els àmbits de comunicació i connectivitat. I, finalment, s'extreuen les conclusions pertinents i es proposen recomanacions per als diferents capítols d'aquest Treball Final de Grau per seguir-lo en un futur.

Table of contents

List of figures

List of tables

List of abbreviations

ADCS   Attitude Determination and Control System

AMS   Asynchronous Messaging Service

AOS   Advanced Orbiting Systems

APL   Johns Hopkins University Applied Physics Laboratory

BSS   Bundle Streaming Service

CFDP   CCSDS File Delivery Protocol

COTS   Commercial Off The Shelf

DOF   Degrees of freedom

DSN   Deep Space Network

DTCP   Delay-Tolerant. Payload Conditioning

DTN   Delay Tolerant Networking

EEIS   End to End Information System

EDL   Entry, Descent, and Landing

ESA   European Space Agency

FDDI   Fiber Distribution Data Interference

FR   Functional Requeriments

IMU   Inertial Measurement Unit

IP   Internet Protocol

ITU   International Telecommunications Union

LILT   Low-irradiance low-temperature

LTP   Licklider Transmission Protocol

MSL   Mars Science Laboratory

NASA   National Aeronautics and Space Administration

OBC   Onboard Computer

RAM   Random Access Memory

RF   Radio Frequency

TCP   Transmission Control Protocol

TFA   Triangular Formation Algorithm

TLR   Top Level Requeriments

TM   Telemetry Protocol

UAV   Unmanned Aerial Vehicle

UDD   User Defined Data

UHF   Ultra-High Frequency

USLP   Unified Space Link Protocol

Symbols list

cm	Centimetre
d	Diameter
h	Hours
Hz	Hertz
v_{ih}	Induced velocity
K	Kelvin
kbps	kilobit per segon
kg	Kilogram
L	Lift
m	Metre
Pa	Pascal
rpm	Revolutions per minute
s	Seconds
T	Thrust
W	Watt
Wh	Watt-hour
W	Weight

Chapter 1

Introduction

1.1   Object

The objective of this project is to design a swarm of Unmanned Aerial Vehicles (UAVs) for the exploration and mapping of Mars, which coordinates with swarms of orbiters and rovers.

1.2   Scope

According to the object of the project, the scope will include the following tasks:

- A preliminary study of a single UAV and its different subsystems.

- An overview of the mission.

- The selection of the Mars location of study based on literature.

- A detailed study of the swarm formation.

- An overview of the multiplatform architecture.

- The delivery of:

    - The project charter.

    - The report.

    - The budget.

    - The quality checklist.

    - The appendices with any additional information considered necessary.

Nevertheless, it will not include the upcoming tasks:

- A specific study of the orbiters and rovers swarms.

- A specific study of any UAV subsystem.

- A specific study to choose the swarm's location of interest.

- The design of the lander of the swarm of UAVs.

1.3 Requeriments

This project must fulfill two different types of requirements to be considered successful: technical and management related. The first group encompasses the engineering requisites to satisfactorily achieve the primary objective of the thesis; while the second group comprises the formatting specification for a correctly deliver of the report.

Technical requirements

- UAV requirements:

  - The UAV shall incorporate the appropriate instruments (sensors and cameras) for the optimal mapping of the Mars surface.

  - For the preliminary study of the propulsion subsystem, two aspects of the Mars environment shall be considered:

    * The planet's atmosphere density is low: approximately 1-2% of Earth's.

    * Martian gravity is approximately 38% of Earth's gravity.

  - For the preliminary study of the thermal subsystem, the average temperatures of the red planet, ranging between $-5°C$ and $-80°C$, shall be considered.

- Swarm requirements:

  - The chosen location where the swarm will perform shall be investigated previously.

  - A base station communication for the UAVs, rovers and satellites swarms shall be established.

  - The convenient algorithm for the UAV swarm flight control and navigation shall be suggested and implemented.

Management requirements

- To write the deliverables mentioned in the scope (1.2) according to the ESEIAAT regulations: the Regulations for the Bachelor Final Thesis [1] and the Final Thesis Procedure [2].

- Prepare slides that complement the bachelor thesis presentation and defense.

- To use the English language to write the deliverables mentioned in the scope (1.2) and during the bachelor thesis presentation and defense.

1.4 Justification

This project is motivated by the increasing interest and technological progress to consider UAVs valuable platforms for planetary exploration [3].

Mars has been a target of human curiosity for hundreds of years. Galileo Galilei was the first person to examine Mars with the aid of a telescope [4] and in the late 1600s skywatchers began to perceive similarities between Earth and the red planet.

From then until now, it has become a planet of great interest for its similarities with Earth, so space agencies and private companies are focusing some of their programs on it.

One of the plans that this bachelor thesis takes into deep consideration is the *Human Exploration of Mars. Design Reference Architecture 5.0* Nasa's book [5], which establishes a long-term plan to explore Mars that breaks down into the following goals:

- Goals I-III: specifies the traditional planetary science goals for understanding Mars' life, climate and geology/geophysics.

- Goal IV: describes the preparation for the first human explorers, which needs a reliable and robust development of exploration systems.

- Goal V: includes the scientific objectives that are unrelated to Mars, such as the ones related to astrophysics, Sun/Moon/Earth observations and the interplanetary environment.

In conclusion, over the last decades, Mars has been explored by orbiting satellites, landed spacecraft and rovers; whiches have limited mobility and provide low-resolution images. Consequently, there is sparse information about the red planet. However, UAVs can overcome this planetary measurement gap because of their numerous benefits: they can map large areas and collect data from different environments, they can obtain better resolution images [3] and they can also rapidly traverse difficult terrain [6]. These benefits applied in a UAV swarm would provide several advantages: rapidity, reliability, diversity and flexibility [7].

Notwithstanding, this project suggests the combination of a constellation of orbiters, a swarm of rovers and a swarm of UAVs to leverage and combine their benefits, mainly focusing on the technical study of the swarm of UAVs.

Chapter 2

State of the art

Mars has been a main target for exploration over the last decades, due to its closeness and similarity to Earth. Since 1975, there have been different programs carried out to explore the surface.

The first program to consider is the Mars Exploration Program [8], which goal consists of the exploration of the red planet and the provision of continuous scientific data through different robotic orbiters, landers and mobile laboratories, such as the Viking 1 and 2, the two Mars Exploration Rovers (Spirit and Opportunity twin rovers), the Mars Science Laboratory (the Curiosity rover), the Mars 2020 (Perseverance Rover and the Ingenuity helicopter), among others.

(a) Viking Lander Model. *Source:*[9]
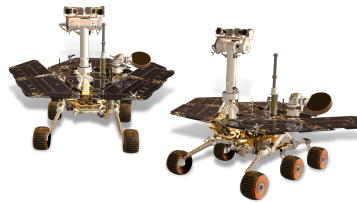
(b) Spirit and Opportunity Model. *Source:*[10]
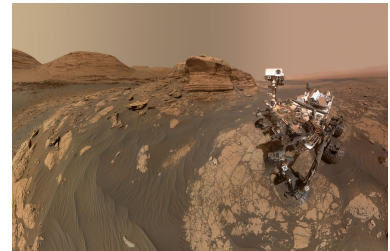
(c) Curiosity rover *Source:*[11]

(d) Perseverance rover *Source:*[12] (e) Ingenuity helicopter *Source:*[13]

Figure 2.1: Mars Expploration Program robotic orbiters, landers and mobile laboratories

Secondly, there is the Discovery Program [15], focused on planetary science missions to enhance a better understanding of the solar system, like the InSight mission on Mars.

Finally, there are other programs to take into consideration, like the Mars Scout [16] (an initiative to send small, low-cost robotic missions to the red planet that was later incorporated into the Discovery Program), the ExoMars [17] (a pair of missions to understand if there was ever life on Mars) [18] or the New

Figure 2.2: Insight lander. *Source:*[14]

Frontiers [19] (which aims to explore the solar system with medium-class spacecraft missions that conduct high-science-return investigations to better understand the Solar System).

2.1 The Ingenuity helicopter

The Ingenuity helicopter, which is part of the Mars 2020 mission [21], is the first aircraft that humanity has sent to another planet to attempt powered and autonomous controlled flight.

During the landing on the red planet on February 18, 2021, specifically on the Jezero Crater area (see figure 2.3), it was located under the belly of the Perseverance rover to have a safe passage to Mars.

Although it was an experimental flight test for technology demonstration, the incorporation of an aerial dimension provides additional mission capabilities that will begin a new era of space exploration [22] .
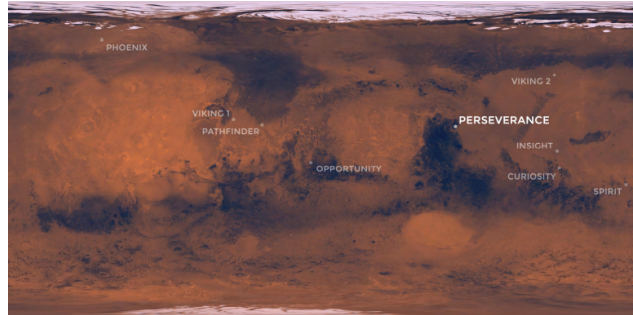
Figure 2.3: Perseverance landing site (Jezero Crater). *Source:*[20]

2.1.1 Specifications of the helicopter

The helicopter itself consists of different subsystems (shown in figure 2.4) and it has the specifications shown in table 2.1.
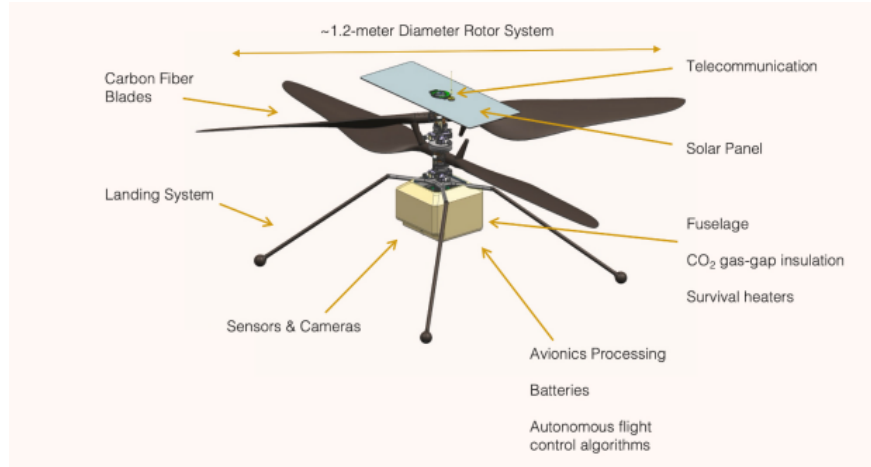
Figure 2.4: Anatomy of the Ingenuity helicopter

Ingenuity specifications	
Weight	1.8 kg on Earth and 0.68 kg on Mars
Height	0.49 meters
Rotor system	4 carbon fiber blades arranged into two 1.2-meter-long counter-rotating rotors that spin at 2,400 rpm
Fuselage (body) dimensions	13.6 cm by 19.5 cm by 16.3 cm
Power	Solar array on top of the rotor system charges 6 lithium-ion batteries

Table 2.1: Ingenuity specifications. *Source:*[20]

2.1.2 Objectives of the helicopter

The primary and most important objective of Ingenuity was to demonstrate rotorcraft flight in the extremely thin atmosphere of Mars. Moreover, the team established several sub-objectives that are listed below [20]:

- Surviving the cruise to Mars and landing on the Red Planet.

- Safely deployment of the helicopter to the surface of Mars from the belly of the Perseverance rover.

- Keeping itself warm through the intensely cold Martian nights.

- Autonomously charging itself with its solar panel.

- Successfully communicating with the Base Station on the Perseverance rover.

- To autonomous operate aerial systems on another planet.

2.2   Dragonfly

The Dragonfly Rotorcraft Lander, which is part of the New Frontiers program, is a multirotor lander to explore numerous high-interest sites on the surface of Titan (Saturn's moon).

The concept of a rotorcraft lander on Titan was proposed 22 years ago, firstly as a helicopter but later as a multirotor drone because of its mechanical simplicity [23].

2.2.1   Spacecraft overview

The Dragonfly has an octocopter (dual quadcopter) design (see figure 2.5) because of the following benefits:

- The rigid, fixed-pich rotors simplify the hub design.

- It reduces the power and torque requirements for a single motor.

- It increases control redundancy.

- The motor/rotor combinations have lowe inertia, which improves the control response.
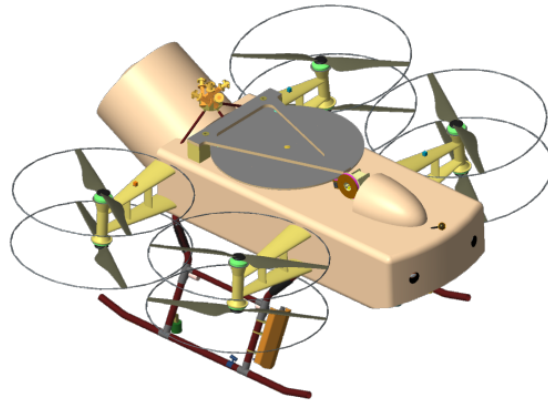
Figure 2.5: Dragonfly configuration. *Source:*[23]

Furthermore, a constraint in this coaxial *X8* configuration that has to be considered is that the rotorcraft must be packaged in a hypersonic aeroshell [24], as shown in figure 2.6.
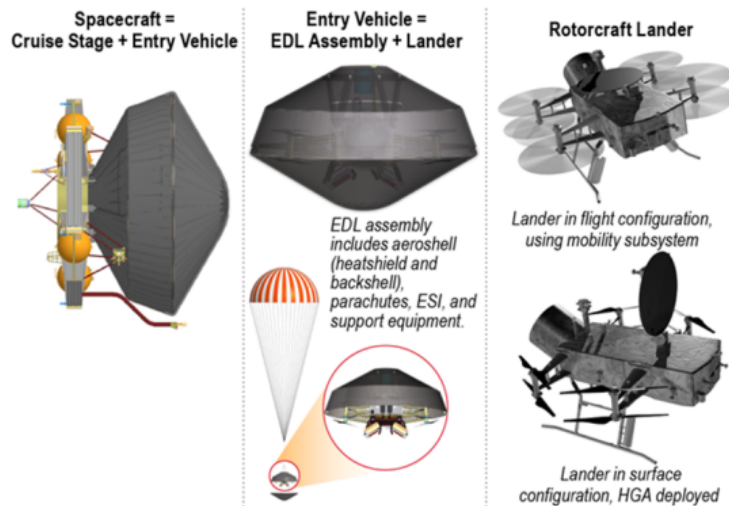
Figure 2.6: Dragonfly spacecraft (left), atmospheric entry vehicle (center), and lander configurations (right). *Source:* [24]

2.2.2 Dragonfly science payload

The Dragonfly science payload incorporates the following instruments:

- **DraMS (Drafongly Mass Spectrometer):** it has a front-end sample processing able to handle high-molecular-weight materials and samples of interest. This system is developed at the Goddard Space Flight Center and includes elements from the successful Sample Analysis on Mars instrument on Curiosity.

- **DraGNS (Dragonfly Gamma-Ray and Neutron Spectrometer):** it allows the determination of the elemental composition of the ground under the lander without requiring sample operations. It is designed at the Goddard Space Flight Center and the Johns Hopkins University Applied Physics Laboratory (APL).

- **DraGMet (Dragonfly Geophysics and Meteorology Package):** it is a combination of simple sensors with low-power data handling electronics designed at the APL.

- **DragonCam (Dragonfly Camera Suite):** it is a combination of cameras that provide forward and downward imaging, developed in the Malin Space Science Systems.

2.2.3 Dragonfly science mission profile

The Dragonfly optical terrain-relative navigation employs two simple operation modes, shown in figure 2.7, and follows the strategy illustrated in 2.8 to choose the new landing sites.
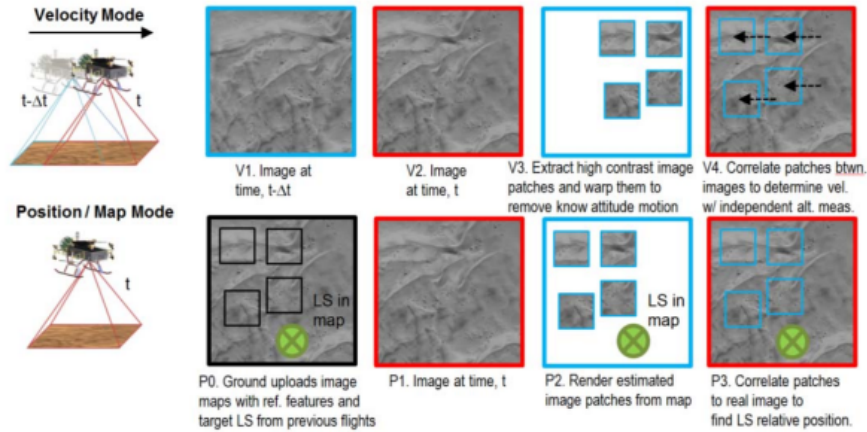
Figure 2.7: Optical navigation modes: optical velocimetry (top), and optical landing site recognition (bottom). *Source:* [24]
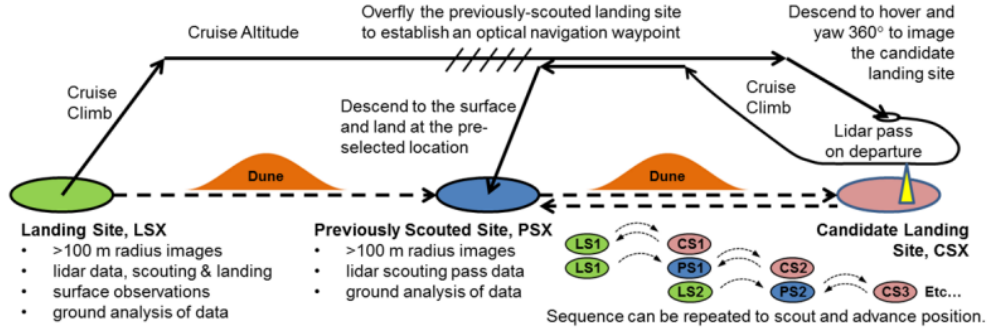
Figure 2.8: Dragonfly illustrative traverse and landing site scouting flight approach. *Source:* [24]

2.3   Swarm configuration

Exploration rovers and orbiters have laid the foundation for the understanding of the red planet. However, they present some limitations in terms of speed and exploration capabilities that the UAVs would overcome because of their additional potential.

As previous and current studies consider [3, 6, 18, 25], UAVs give a new perspective of a region's geology and permit access to rugged terrain, provide high-definition images and could rapidly traverse large distances. Moreover, in future missions, they could collect samples, carry instrument payload for in-situ scientific investigation or act as a supporting platform for rovers.

Therefore, the present bachelor's final thesis not only will combine rovers, orbiters and UAVs for a Mars mapping mission to leverage its benefits, but will also study and suggest that each of them behaves in a swarm configuration, mainly focusing on the UAVs swarm. This type of configuration increases reliability, availability, speed and range, and it is cost-effective compared to a single robotic mission [7].

Chapter 3

Theoretical background

3.1 UAV definition

A UAV is a fixed-wing, rotor-wing, or lighter-than-air vehicle designed to be operated through electronic inputs initiated by the flight controller or by an on-board autonomous flight management control system.

3.2 Configuration of the UAV

3.2.1 UAV configuration types

There are different types of UAV classifications, either according to their range of action, size and payload, levels of autonomy, or their aerodynamic configuration (see figure 3.2). Considering the aerodynamic configuration classification and focusing on the rotary-wing subclass, further classification is found [26] (see figure 3.1):

- Single-rotor

- Coaxial

- Quadrotor

- Multi-rotor

(a) Single-rotor. *Source:*[27] (b) Coaxial. *Source:*[28] (c) Quadrotor *Source:*[29] (d) Multi-rotor *Source:*[30]

Figure 3.1: UAV configuration types.
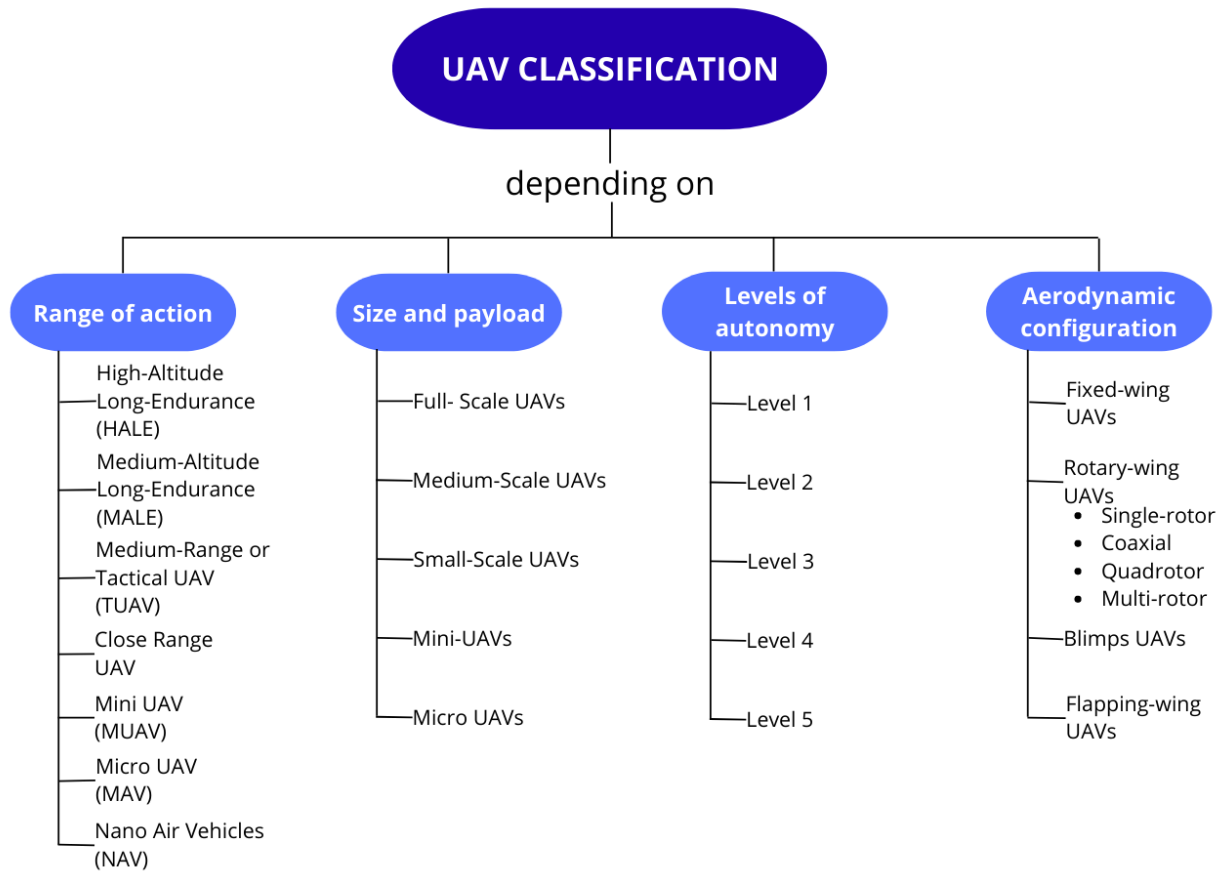
Figure 3.2: UAV configuration types. *Source:* [26]

Table 3.1 compares different aircraft configurations based on distincs concepts. As it can be noticed, the coaxial rotor and the quadrotor offer the best performance.

Configuration	A	B	C	D	E	F	G	H
Power cost	2	2	2	2	1	4	3	3
Control Cost	1	1	4	2	3	3	2	1
Payload/volume	2	2	4	3	3	1	2	1
Maneuverability	4	2	2	3	3	1	3	3
Mechanics simplicity	1	3	3	1	4	4	1	1
Aerodynamics Complexity	1	1	1	1	4	3	1	1
Low Speed Flight	4	3	4	3	4	4	2	2
High Speed Flight	2	4	1	2	3	1	3	3
Miniaturization	2	3	4	2	3	1	2	4
Survivability	1	3	3	1	1	3	2	3
Stationary Flight	4	4	4	4	4	3	1	2
TOTAL	24	28	32	24	33	28	22	24

Table 3.1: Aircraft comparison (1=Bad, 4=Very good; A=Single rotor, B=Axial rotor, C=Coaxial rotors, D=Tandem rotors, E=Quadrotor, F=Blimp, G=Bird-like, H=Insect-like). *Source:*[31]

3.2.2   Selection of the configuration

According to the results given in table 3.1 and the following arguments, the selected configuration of the UAV is the coaxial quadrotor.

- It is more appropriate for a Martian mission. It can be customized to produce the necessary Mach and chord Reynolds numbers to have an efficient airfoil opperation in restrivtive Martian conditions. Moreover, it is suitable for compact stowage [32].

- Its technology is more mature [32].

- It is efficient in terms of the thrust produced and the occupied space [33].

- It generates more thrust, which allows to carry more payload (such as cameras or navigation devices that are required for the mission) [34].

- It is more resilient, so it could tolerate the loss of at least one rotor or motor [23]. Thus, a relevant space agency as the National Aeronautics and Space Administration (NASA) has chosen this configuration for its Dragonfly project (section 2.2).

3.2.3   UAV modelling

The concept

The coaxial quadrotor concept is the same as the quadrotor. Its control is achieved by the speeds of eight rotors $(\Omega_1, \Omega_2, \Omega_3, \Omega_4, \Omega_5, \Omega_6, \Omega_7, \Omega_8)$ and the direction of rotation of each rotor is illustrated in figure 3.3:
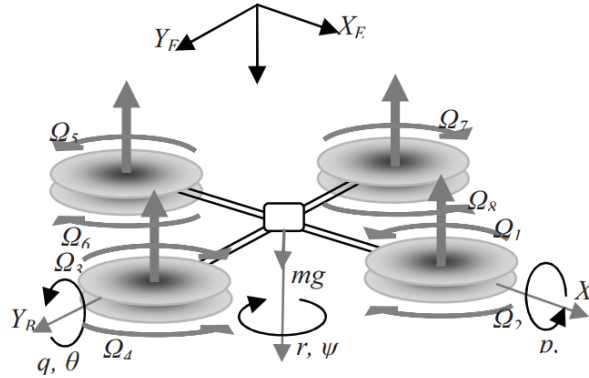
Figure 3.3: Dynamics and concept of coaxial quadrotor. *Source:* [34]

The overall speeds $(\Omega, \text{rad/s})$ generation is represented by equation 3.1:

$$\Omega = -\Omega_1 + \Omega_2 - \Omega_3 + \Omega_4 - \Omega_5 + \Omega_6 - \Omega_7 + \Omega_8 \tag{3.1}$$

Furthermore, each thrust value is assumed to be equal and the yawing motion is assumed to be stable even though the dynamics of the quadrotor produce an unstable system [34]. Thereby, the vector of movement is represented in equation 3.2:

Vector of movement

$$
\begin{cases}
U_1 = b \sum_{i=1}^{8} \Omega_i^2 \\
U_2 = l\, b\, (\Omega_7^2 + \Omega_8^2 - \Omega_3^2 - \Omega_4^2) \\
U_3 = l\, b\, (\Omega_5^2 + \Omega_6^2 - \Omega_1^2 - \Omega_2^2) \\
U_4 = d\, (\Omega_2^2 + \Omega_4^2 + \Omega_6^2 + \Omega_8^2 - \Omega_1^2 - \Omega_3^2 - \Omega_5^2 - \Omega_7^2)
\end{cases}
\tag{3.2}
$$

where U_1 is throttle, U_2 is roll, U_3 is pitch, U_4 is yaw, l (m) is the distance between the center of the coaxial rotor and the center of a propeller, b (Ns^2) is the thrust coefficient and d (Nms^2) is the drag coefficient.

Equations of motion

The following premises have been assumed [34] to describe the 6-DOF (Degrees of freedom) equation (using the Newton-Euler concept):

- The coaxial quadrotor is a rigid-body.

- The center of mass coincides with the origin of the body-fixed frame.

- The coaxial quadrotor has symmetric dimension.

- The axes of the body frame coincide with the inertial coordinate system.

Eqs. (3.3) to (3.5) illustrate the translational dynamics in the coaxial quadrotor, where g (m/s^2) is the gravity force and m (kg) is the overall coaxial quadrotor mass.

$$
\ddot{x} = (\, sin\psi\ sin\phi\ +\ sin\psi\ sin\theta\ cos\phi)\ \frac{U_1}{m}
\tag{3.3}
$$

$$
\ddot{y} = (\, -\ cos\psi\ sin\phi\ +\ sin\psi\ sin\theta\ cos\phi)\ \frac{U_1}{m}
\tag{3.4}
$$

$$
\ddot{z} = -g + (sin\theta\ cos\phi)\ \frac{U_1}{m}
\tag{3.5}
$$

Eqs. (3.6) to (3.8) show the rotational dynamics of the coaxial quadrotor, where I_{XX}, I_{YY}, I_{ZZ} are the moments of inertia of each axis, J_{TP} (Nms^2) is the total rotational moment of inertia, p, q and r are the components of Ω and $\ddot{\varphi}$, $\ddot{\theta}$ and $\ddot{\psi}$ are the roll, pitch and yaw accelerations.

$$
\ddot{\varphi} = (\, p\, q\, (I_{XX} - I_{YY}) + U_4)\ \frac{1}{I_{ZZ}}
\tag{3.6}
$$

$$\ddot{\theta} \; = \; (\, p\, r\, (I_{ZZ} \; - \; I_{XX}) \; - \; J_{TP}\, p\, \Omega \; + U_3)\, \frac{1}{I_{YY}} \tag{3.7}$$

$$\ddot{\psi} \; = \; (\, p\, r\, (I_{ZZ} \; - \; I_{XX}) \; - \; J_{TP}\, p\, \Omega \; + U_3)\, \frac{1}{I_{YY}} \tag{3.8}$$

3.3   Mission needs

This section presents relevant datum for the understanding of Mars and the challenges that the UAV would overcome to do a satisfactory performance.

3.3.1   Mars parameters

Mass (kg)	$6.42 \cdot 10^{24}$
Diameter (km)	6792
Density (kg/m^3)	3.93
Gravity (m/s^2)	3.71
Rotation period (h)	24.6
Length of Day (h)	24.7
Orbital period (days)	687.0
Orbital velocity (km/s)	24.1
Surface Pressure (bars)	0.01

Table 3.2: Mars parameters. *Source:*[35]

3.3.2 Martian atmosphere parameters

Surface pressure (Pa)	636
Surface density (kg/m^3)	0.020
Scale height (km)	11.1
Total mass of the atmosphere (kg)	$2.5 \cdot 10^{16}$
Average temperature (K)	210
Diurnal temperature range (K)	184 to 242
Wind speeds (m/s)	summer: -7
	fall: 5-10
	dust storm: 17-30

Table 3.3: Martian atmosphere parameters. *Source:*[35]

3.3.3 Martian temperatures

The estimation of Mars temperatures in terms of altitude follows the mathemathical model provided by NASA Jet Propulsion Laboratory (JPL), which is based on the Mars Global Reference Atmospheric Model (Mars-GRAM) [36]. The temperature equation shown in 3.9 was generated for a latitude of -20 and provides data from the surface to an altitude of 10 km.

Thus, figure 3.4 illustrates Martian temperatures for different altitudes, and table 3.4 summarizes temperature values in 4 different areas of the red planet.

$$T(h) = 238.74 - 34.488h + 35.133h^2 - 15.96h^3 + 3.7315h^4 - 0.47352h^5 + 0.030962h^6 - 0.000817h^7 \quad (3.9)$$
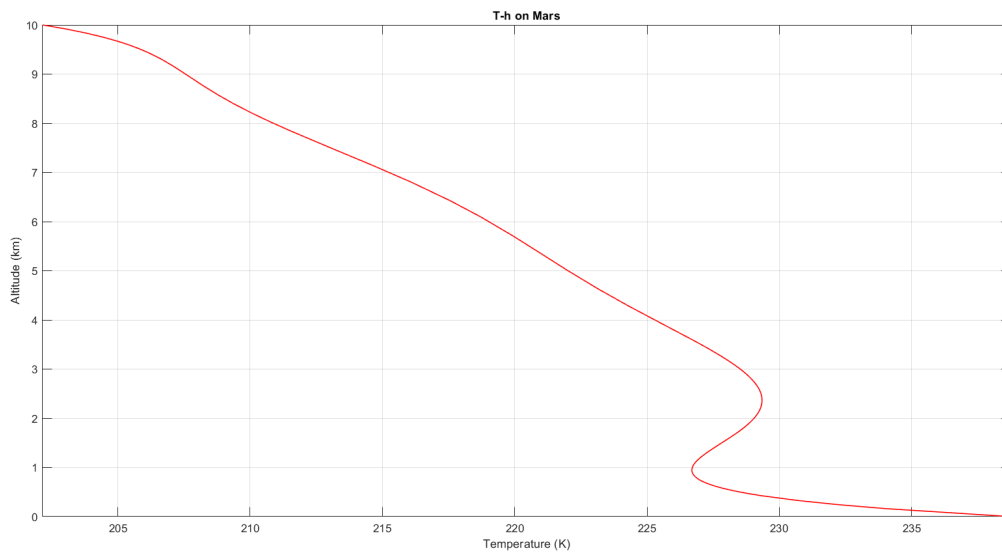
Figure 3.4: h-T on Mars. *Source: own elaboration based on* [36]

Zone	Altitude (km)	Temperature (K)
North polar cap	2.5-3.0	228.5-229.3
South polar cap	1.0-3.5	226.7-227.0
Equator	0	238.7
Cydonia Mensae	0.1-0.65	227.4-235.6

Table 3.4: Martian temperatures. *Source:*[37, 38]

Chapter 4

Mission definition

4.1 The mission

According to the design cycle of the European Space Agency (ESA), this project encompasses until the Preliminary Design Review of the mission (PDR).
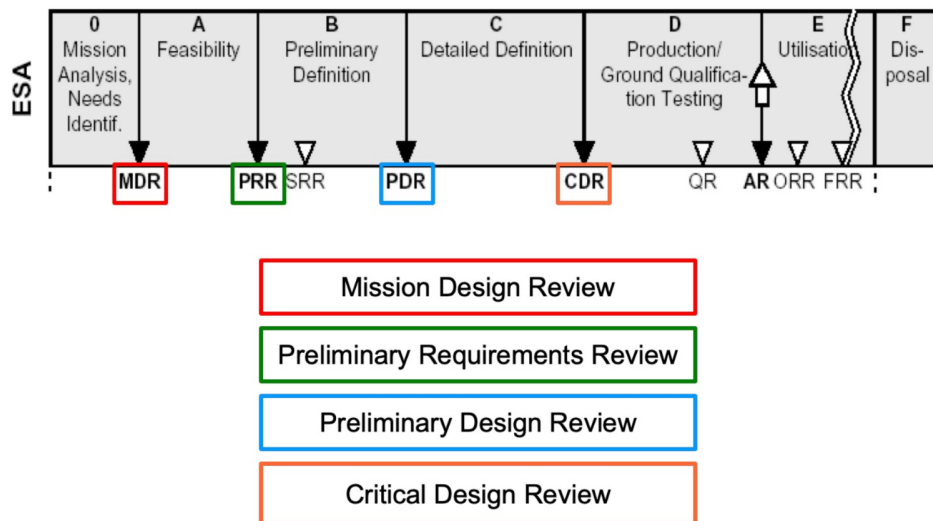
Figure 4.1: Levels of design of a mission according to ESA. *Source:*[39]

4.1.1 Mission statement

Mars has been a primary target for exploration over the last decades due to its closeness and similarity to Earth. Exploration landers and rovers have laid the foundation for the understanding of the red planet, however, they present some limitations that UAVs would overcome. In consequence, this project aims to design a swarm of UAVs to provide a new perspective for planetary exploration and search for suitable caves for a future permanent settlement.

4.1.2 Mission approach

For this mission, the swarm of UAVs will cooperate with an existing constellation of satellites and a swarm of rovers to explore a specific area of Mars.

4.1.3 Primary objectives

- To demonstrate the capability of UAVs formation flight.

- To demonstrate the cooperation feasibility of a swarm of UAVs and the existing swarm of rovers and satellites constellation.

- To detect caves that are likely to be viable sites for future Mars missions and future Martian bases.

4.1.4 Secondary Objectives

- To complement the satellite's research on regions that are thought to have hosted water in the past.

- To obtain images for general distribution to gain public support for space exploration.

4.1.5 Mission requirements

The mission requirements, whiches determine the expectations of the suggested mission in a quantifiable, consistent, unambiguous and traceable way, are listed on the next page, in table 4.1.

The proposed requirements are divided into the following categories:

- **TLR (Top Level Requirements):** they define the goal of the mission.

- **FR (Functional Requirements):** they are necessary elements and characteristics to accomplish the TLRs.

- **CR (Critical Requirements):** they define the development of the overall mission, determining its success or failure. They have been marked in bold.

Furthermore, the second part of the ID corresponds to the Mission Design (in the case of the initialism MD) or the different subsystems of the UAV:

- PAS: Payload Subsystem.

- PRS: Propulsion Subsystem.

- ADCS: Attitude Control and Determination System.

- NS: Navigation Subsystem.

- PES: Power and Energy Subsystem.

- TS: Thermal Subsystem.

- LS: Landing Subsystem.

- CS: Communications Subsystem.

- SS: Structural Subsystem.

- OBCS: Onboard Computer Subsystem.

ID	Requirement description	Last updated
TLR-01	**The swarm of UAVs shall be gently deployed on the surface of Mars.**	**11/22/22**
	Mission Design	
FR-MD-01	**Two (TBC) one-way cargo trips shall be performed in order to deploy the swarm of 3 (TBC) UAVs on the surface of Mars.**	**11/22/22**
FR-MD-02	The UAVs shall weigh less than 8kg (TBC).	11/22/22
FR-MD-03	The airframe diameter of the UAVs shall be less than 1m (TBC).	11/22/22
	Payload Subsystem	
FR-PAS-01	A measurement and object detection system shall be incorporated to map 3 dimension areas.	11/22/22
FR-PAS-02	An instrument for obtaining images shall be selected to gain public support for space exploration.	11/22/22
	Propulsion Subsystem	
FR-PRS-01	**A propulsion generator system capable of generating lift shall be selected and designed.**	**11/22/22**
FR-PRS-02	The optimal and most resilient configuration of the propulsion generator system shall be decided.	11/22/22
	ACDS Subsystem	
FR-ACDS-01	**Attitude determination control instruments shall be selected to guarantee an optimal performance of the UAV.**	**11/22/22**
	Navigation Subsystem	
FR-NS-01	**Navigation instruments shall be chosen in order to provide graphical coordinates and directions for the UAV.**	**11/22/22**
FR-NS-02	Redundant navigation instruments shall be considered to ensure the navigation of the UAV on Mars.	11/22/22
	Power and Energy Subsystem	
FR-PES-01	**A power generation system capable of generating electrical power shall be provided during the whole mission.**	**11/22/22**
FR-PES-02	An energy storage system shall be provided to supply electrical power when the power generation mechanisms are not active.	11/22/22
	Thermal Subsystem	
FR-TS-01	**A thermal generator system capable of protecting the avionics from the cold environment of Mars shall be selected to ensure the optimal performance of the UAV.**	**11/22/22**
FR-TS-02	Appropriate fuselage outer-layer material/s (with a high thermal absorptivity and low emissivity) shall be selected in order to harvest ambient solar thermal energy during the day to warm the UAV and minimize thermal radiative losses at night.	11/22/22
	Landing Subsystem	
FR-LS-01	A landing system mechanism capable of preventing itself from digging into soft landing surfaces shall be selected.	11/22/22
FR-LS-02	Appropriate materials for the landing system mechanism shall be selected in order to ensure successful landings.	11/22/22
	Communications Subsystem	
FR-CS-01	The overall mission communication architecture shall be designed in order to allow communication between the swarm of UAVs, the swarm of rovers and the orbiters constellation.	11/22/22
FR-CS-02	A communication system that allows communication between the UAV and the next element of another swarm shall be selected.	11/22/22
	Structural Subsystem	
FR-SS-01	Appropriate materials for the structural resistance of the UAV shall be selected.	11/22/22
FR-SS-02	The deployment of the UAV shall be defined to study if some folding mechanisms are needed.	11/22/22
	OBC Subsystem	
FR-OBCS-01	A preliminary study of the required On-Board Computer of the UAV shall be carried.	11/22/22

Table 4.1: Mission requirements. *Source:* Own elaboration

4.2 Location

The selection of the location of study for this mission is based on literature [40, 41, 42, 43] and the interest of the area considered, Cydonia Mensae (see figure 4.2), over the years.

Figure 4.2: Cydonia Mensae location. *Source:*[44]

As it is widely known, numerous unexplored Martian regions are of high potential interest. In the case of the Cydonia Mensae area, it has only been observed by the Viking 1 and the Mars Express. However, this region has considerable interest because it is thought to have hosted seas or lakes in the past, whiches later were covered by lava and sediment deposits.

The dominant morphologic features are the followings:

- **Clusters of large massifs and plateau outliers:** they are remains of cratered material which probably consist of flat-lying beds of eolian sediment and lava. The majority are less than 5 km wide, although they may be as wide as 10 km.

- **Knobs:** they are considered to be remnants of the underlying cratered terrain or igneous intrusions. Most are about 2 km across.

- **Smooth lowland plains:** they are arcuate to linear ridges, surround the clusters and link different isolated knobs. Their widths vary from 100 m to 2 km and their length is typically from 5 to 10 km [43, 41].

Overall, it may be declared that rovers might not provide enough details due to the nature of Cydonia Mensae (valleys, debris and craters are hard to explore). However, they could play a significant role in surface exploration.

4.3 The swarm

The mission is based on the assumption that swarms are suitable to solve complex problems combining simple tasks and behaviours. That is, a group of single components cooperate and produce significant results by combinig elementary performances to achieve ambitious goals. Moreover, the common goal would be divided into scondary goals that each swarm would accomplish.

Overall, swarms have the potential to change future space exploration missions because of their resiliency, adaptability and low-cost multi-agent systems; and the principal enabling technologies are cooperation (based on manipulation, motion planning and task recognition/allocation) and formation keeping [40, 45, 46].

4.3.1 Orbiters constellation

The orbiters constellation would provide widespread and continuous coverage of the location of study due to the multiple angles and multipoint observations, both of which are crucial for the scientific understanding of the Cydonia Mensae area.

The first mapping would enable a general vision of the surface and the detection of the subareas of interest that the UAVs swarm would explore. For example, difficult access areas or specific sediments.

Therefore, the Mars Express orbiter [47] is one of the orbiters that form the selected constellation, the Mars Relay Network, because it has provided the most complete and accurate coverage of the surface, subsurface and atmosphere of the red planet. It consists of a 3-axis stabilized orbiter with a fixed high-gain antenna and body-mounted instruments, and it is placed in an elliptical orbit (250 x 10142 km) of 86.35°quasi-polar inclination with a 6.75 h period.

The orbiter, which is part of the first European mission to any planet, launched in June 2003 from the Baikonur Cosmodrome in Kazakhstan aboard a Russian Soyuz rocket, entered Mars orbit on 25th December 2003 and nowadays is still active.

Figure 4.3: Mars Express spacecraft. *Source:* [48]

Moreover, it has the following scientific instruments:

- Super/High-Resolution Stereo Colour Imager.

- Visible and Infrared Mineralogical Mapping Spectrometer.

- Atmospheric Fourier Spectrometer.

- Subsurface-Sounding Radar/Altimeter.

- Energetic Neutral Atoms Analyzer.

- Ultraviolet and Infrared Atmospheric Spectrometer.

- Radio Science Experiment.

Thus, the chosen constellation includes four more satellites that would also take part in this mission for communication purposes (see section 7.1.1 for more information). So, the overall swarm is comprised of 5 orbiters: the Mars Express orbiter, the Mars Reconnaissance Orbiter, the Mars Atmospheric and Volatile EvolutioN, the Mars Odyssey and the ExoMars Trace Gas Orbiter.

4.3.2 UAVs swarm

The UAVs swarm would conduct a more specific investigation of the areas of interest, considering the information of the orbiters constellation to better search caves for future Mars missions. However, drone autonomy is a crucial restraint to take into account while researching the red planet's surface.

Furthermore, the swarm would provide higher-resolution images that would give a better knowledge of the studied areas and they would be also distributed to the general public to increase the general interest in space exploration. Section 6 deeply describes the swarm of UAVs.

The lander

The lander is a spacecraft that carries the UAVs to Mars in order to protect them during the entry, descent and landing on the red planet, so it has to be both strong and lightweight. Based on these requeriments, its preceding performance and its architecture, and considering 3 UAVs for the swarm (for algorithm simplifications and for being an appropiate number of vehicles to study the Mars surface), the selected lander for this mission is the Mars Science Laboratory (MSL) [49, 50, 51], which successfully landed the Curiosity rover [4, 52] on the surface of the red planet in 2012.

The MSL incorporated the MSL Entry, Descent, & Landing Instrument suite (MEDLI), a combination of sensors that measured the atmospheric conditions of the entry heatshield of the MSL during the atmospheric entry and descent and provided relevant engineering data for the design of entry systems of the following planetary missions.
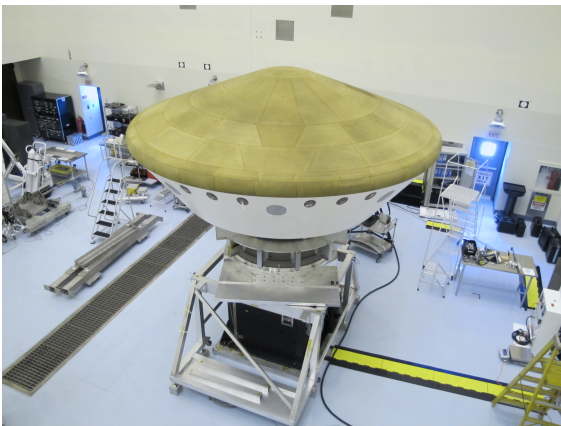
(a) Mars Science Laboratory (MSL). *Source:* [53]
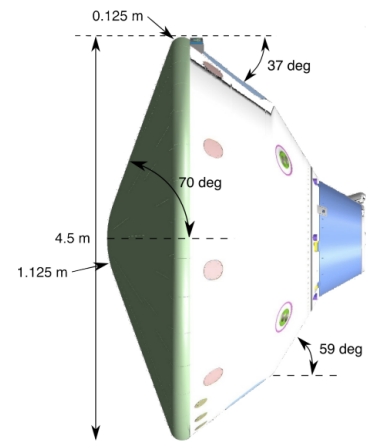
(b) Mars Science Laboratory (MSL) geometry. *Source:* [50]

Figure 4.4: The lander

As figure 4.4 illustrates, its size is enough to carry the 3 swarms, which would reduce the cost of the mission. However, although sending the overall swarm in one lander is risky, taking into consideration that only about 60% of the missions sent to Mars are successful, it is considered that the appropiriate and successful performance of the MSL during the Curiosity and Perseverance rovers guarantees the selection of this lander.

Finally, figure 4.5 shows the Entry, Descent, and Landing (EDL) maneuver [54] completed by the lander that carried the Perseverance rover (the MSL) to the surface of Mars, which is the same that the mission suggested in this bachelor final thesis would make.

The EDL is a short but also intense and hard phase of a Mars mission. In particular, only about 40%[54] of the overall missions ever sent to Mars by any space agency have landed successfully. Furthermore, another restraint to take into consideration is that the radio signal during the landing on the surface of Mars is received with a 11 minutes delay. So, the lander is designed to complete the entire EDL process, also known as the "Seven Minutes of Terror", autonomously.
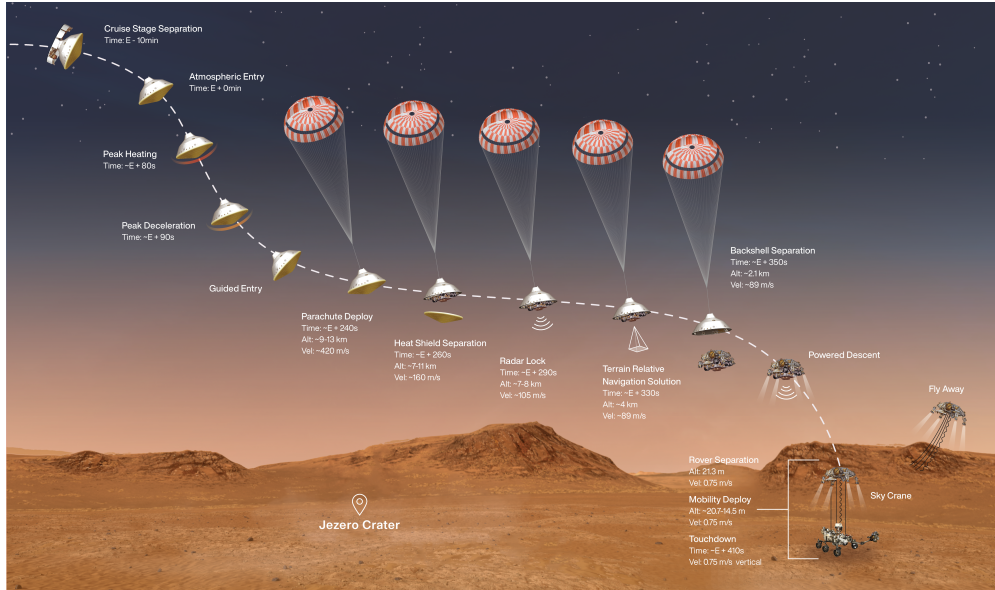
Figure 4.5: Perseverance Rover's Entry, Descent and Landing Profile in the final minutes. *Source: [55]*

Thus, the EDL process can be schematized as:

- **Final Preparations:** 10 minutes before entering the atmosphere, the spacecraft removes its cruise stage, so that only the protective aeroshell (with the UAVs and descent stage inside) lands on the surface of Mars. Moreover, the vehicle reorients itself before entering the atmosphere of the red planet.

- **Atmospheric Entry:** the drag forces slow down the spacecraft when entering the atmosphere, but they also raise dramatically its temperature. Furthermore, the spacecraft fires small thrusters to adjust the angle and direction of lift as it descends through the atmosphere.

- **Parachute Deployment:** using the Range Trigger technology, the spacecraft calculates the ideal time to open the parachute.

- **Focusing on Landing:** 20 seconds after the parachute deployment, the heat shield separates from the spacecraft and the coverage of the UAVs is exposed to the atmosphere of Mars. Meanwhile, the Terrain-Relative Navigation technology is used to choose the safest spot to land.

- **Powered Descent:** the parachute is removed and the powered descent stage fires up its engines to avoid the impact by the parachute and ensure a safe landing on the surface of Mars.

- **Skycrane Maneuver:** finally, 12 seconds before the landing, a set of cables lowers the coverage of the UAVs. When it touches down the ground, the cables are cut and the descent stage lands uncontrolled on the surface in a safe distance.

4.3.3   Rovers swarm

The swarm of rovers would be the last element of the overall swarm, so its performance depends on the previous work done by the orbiter constellation and the swarm of UAVs. Hence, the studied areas by the swarm of UAVs would prepare the selection of distinguished points of interest for a profound study done by the swarm of rovers and, also, the research on regions that are thought to have hosted water in the past. Besides, the rover leader of the swarm acts as the base station communication between the UAV leader and Earth. Thus, the selected rovers for this swarm are the same designs as the Perseverance rover (see figure 4.6), considering that one of its spectrometers allows a more detailed chemical analysis of elements than ever before. Furthermore, the other

Figure 4.6: Perseverance rover on Mars. *Source:[56]*

instruments are a mixture of upgraded versions of Curiosity rover instruments and new ones [57, 58, 59]:

- Mastercam-Z: it's an advanced camera system to understand the geologic structures of the red planet.

- MEDA (Mars Environmental Dynamics Analyzer): it consists of a set of sensors to measure temperature, wind speed and direction, pressure, relative humidity and dust size and shape.

- MOXIE (Mars Oxygen ISRU Experiment): it's an oxygen processing plant intended to support a human expedition in the 2030s.

- PIXL (Planetary Instrument for X-ray Lithochemistry): its role consists of determining the elemental composition of Martian surface materials.

- RIMFAX (Radar Imager for Mars' Subsurface Experiment): it provides a centimeter-scale resolution of the geologic structure of the Mars subsurface.

- SHERLOC (Scanning Habitable Environments with Raman & Luminescence for Organics and Chemicals): it is a spectrometer that determines fine-scale mineralogy and detects organic compounds.

- SuperCam: its role consists of taking images, analyzing chemical composition, studying minerals and recording audio.

Chapter 5

Single UAV overview

5.1 UAV subsystems

5.1.1 Payload

This section comprises the necessary instruments that the UAV requires for scientific research on the Mars surface.

- **Camera:** a one color 13 megapixel horizon-facing terrain camera, with a global shutter, on the bottom of the fuselage to acquire color images during flight that later can be distributed to the general public [22].

- **Image processing chip:** it is a processor designed to support sharper image capture, provide faster processing and more advanced connectivity.

- **LiDAR (Light Detection and Ranging o Laser Imaging Detection and Ranging) sensor:** it is a measurement and objects detection system based on laser technology to represent surfaces and map 3 dimensions areas. Particularly, its scanner emits infrared laser beams that impact certain objects and bounces (see figure 5.1). Then, the receiver registers the bounced beams and measures the distance. This type of sensor builds terrain models with 1-2 cm accuracy and does not require additional processing [60].
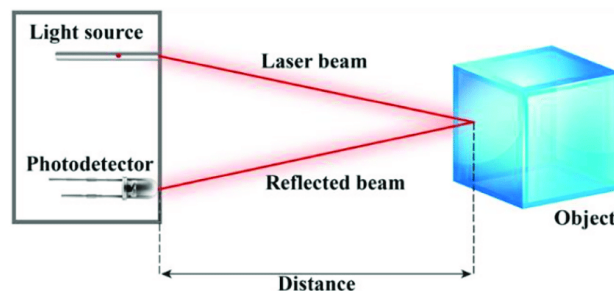
Figure 5.1: LiDAR sensor functioning scheme. *Source:*[61]

5.1.2 Propulsion Subsystem

Propeller efficiency and motor reliability are two constraints to take into account when designing a Mars multirotor.

So, this subsection is based on the high-speed brushless motors for the Martian applications study [62], which presents a summary of work performed to qualify two COTS (Commercial Off The Shelf) industrial standard motor types,(a $\emptyset$13 mm brushed motor and a $\emptyset$22 mm brushless one), in order to lower development costs. From its results, the brushed motor is dismissed because its expected lifetime is lower than the brushless motors and the common brush materials require the presence of water vapor and oxygen. Moreover, results illustrate that the $\emptyset$22 mm brushless motors can work at temperatures between 218.15 K and 313.15 K and at rotation speeds of up to 12,000 rpm. Consequently, this bachelor's final thesis considers a minimum value of 11,000 rpm to guarantee the viability of the selected design.

Furthermore, the following assumptions are made in order to estimate the value of particular parameters, whiches are based on [40] because it proposes a design of a UAV that has similar order of magnitude and requirements:

- Flight endurance: 30 min

- Total mass of the UAV: 8 kg

Thus, the preliminar weight, thurst and drag are estimated below:

- Weigh (W):
$$W = 7kg \cdot 3,71 \, \frac{m}{s^2} \; \rightarrow \; \boxed{W = 25.97 \, N} \tag{5.1}$$

- Thrust (T): in hover T=W so,
$$T_T = W \rightarrow \boxed{T_T = 25.97 \, N} \tag{5.2}$$

- Diameter (d): in hover, the diameter can be calculated from the induced velocity (v_{ih}) at rotor disk in hover flight,
$$v_{ih} = \sqrt{\frac{W}{2\rho \cdot \frac{\pi}{4} \cdot d^2}} \tag{5.3}$$

The value of the induced velocity is estimated to be in the same magnitude order as the one in [40], so it is calculated as
$$v_{ih} = \sqrt{\frac{W}{2\rho \cdot \frac{\pi}{4} \cdot d^2}} = \sqrt{\frac{19.6}{2 \cdot 0.020 \cdot \frac{\pi}{4} \cdot 0.30^2}} = 83.26 \, m/s \tag{5.4}$$

Consequently, the estimated diameter is calculated as follows:
$$v_{ih} = \sqrt{\frac{W}{2\rho \cdot \frac{\pi}{4} \cdot d^2}} = \sqrt{\frac{25.97}{2 \cdot 0.020 \cdot \frac{\pi}{4} \cdot d^2}} = 83.26 \rightarrow \boxed{d = 0.31 \, m} \tag{5.5}$$

Finally, table 5.1 summarizes the reference configurations of the Propulsion Subsystem. As they are in the same magnitude order as the ones in [40], they are accepted as preliminary reference configuration values.

Diameter (m)	0.31
Total mass (kg)	8.0
Flight endurance (min)	30
Rotating speed (rpm)	11,000
Weight on Mars (N)	2.,97
Thrust$_{\textbf{hover}}$(N)	25.97

Table 5.1: Propulsion Subsystem reference configurations. *Source:* Own elaboration

5.1.3 ADCS

The Attitude Control and Dettermination System (ADCS) is responsible for controlling and determining the orientation of the UAV and the essential sensors required to achieve it are the followings:

- **IMU (Inertial Measurement Unit):** for measuring accelerations and angular rates in three directions. It is a combination of an accelerometer (to measure speed and linear acceleration/force) and a gyroscope (to provide a measure of the angular rate). *Figure 5.2 shows the 6 DOF.*

- **Inclinometer:** it consists of 2 accelerometers that only measure gravity before the spin-up and the take-off to calibrate the IMU accelerometer biases.

- **Laser rangefinder** (included in the LiDAR sensor)**:** to measure the distance to the ground (see figure 5.3). The Ingenuity helicopter and the Dragonfly UAV also use it because of its lightness, high intensity, acuteness to calculate very small but also large distances, very high precision and sharp focus on small surfaces.
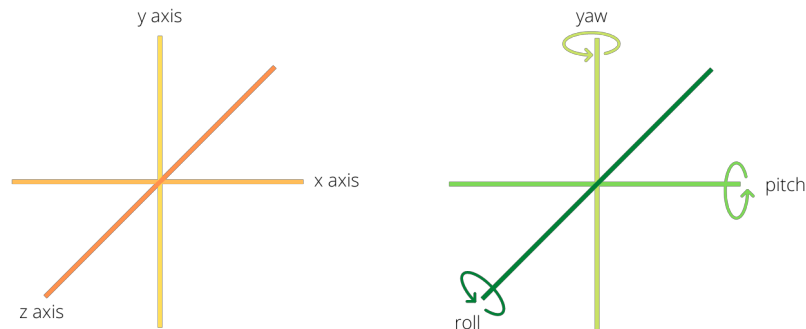
Figure 5.2: The six degrees of freedom *Source:* own elaboration
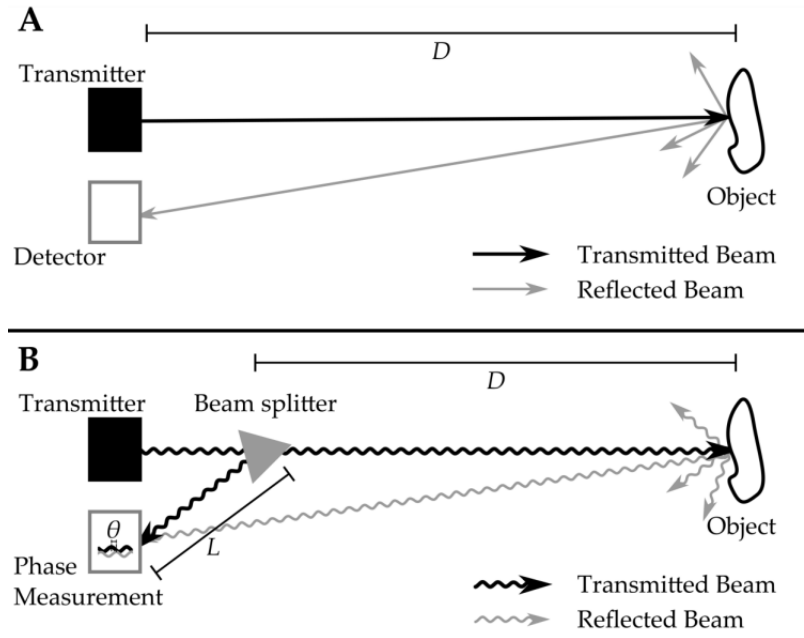
Figure 5.3: Laser rangefinder functioning scheme *Source:* [63]

5.1.4 Navigation Subsystem

The Navigation Subsystem assists navigation in the UAV and it basically consists of the following instruments [20, 22, 64]:

- **Navigation camera:** one black-and-white 0.5-megapixel downward-facing navigation camera located on the bottom of the fuselage for navigation purposes (to determine position, attitude, velocity and other variables).

- **System on a chip:** it is an integrated circuit that stores the components of the electronic navigation system. This processor controls the visual navigation algorithm via a velocity estimation taking into account the terrain features tracked with the navigation camera.

- **2 flight-control microcontroller units (MCUs):** they are small integrated circuits, in witches the system on a chip is connected, that are required to perform certain flight-control functions.
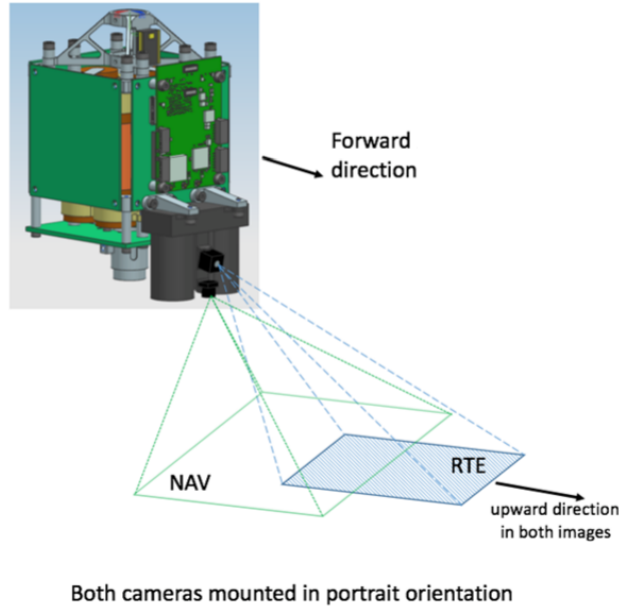
Figure 5.4: Navigation (NAV) and payload (RTE) cameras functioning scheme.*Source:*[65]

5.1.5 Power and Energy Subsystem

The Power and Energy Subsystem is essential for the performance of the UAV because it not only generates the electrical power it needs during its flights (supporting both the platform and the payload) but also provides the required energy for its survival on Mars. Therefore, this subsystem is critical in the design and operation of the UAV.

Power consumption

The preliminar power consumption is estimated from the preliminar thrust result calculated in section 5.1.2:

$$P \;=\; 2\rho \cdot \frac{\pi}{4} \cdot d^2 \cdot v_{ih} \;=\; 2 \cdot 0.020 \cdot \frac{\pi}{4} \cdot 0.31^2 \cdot 83.26^3 \;\rightarrow\; \boxed{P \;=\; 1742.5\,W} \tag{5.6}$$

The batteries

When choosing the most suitable batteries for the UAV, the following constraints shall be taken into account:

- dimension.

- mass.

- survival and performance on Mars.

- specific energy.

- self-discharge.

Consequently, the SAFT VES180 cells [66] have been considered. These Lithium-Ion cells are a type of rechargeable batteries that use the reduction of lithium ions to store energy. Compared to other materials, they offer high energy densities, low self-discharge and no memory effect [1] Moreover, they have been used in previous exploration rovers (such as the Pathfinder), which demonstrates their survivability under Mars conditions.

Compared to NiH_2 batteries (see figure 5.2 for competitors comparison), the Li-ion ones offer a higher specific energy (more of 40 % weight reduction), higher Faradaic efficiency [2] and lower self-discharge (0.03 % compared to 10 %).

	NiCd	NiH2	Li-Ion	System Impact
Energy Density (Wh/kg)	30	60	125	Weight Saving
Energy Efficiency %	72	70	96	Reduction of charge power: solar panel
Thermal Power (Scale: 1-10)	8	10	3	Reduction of radiator, heat pipes sizes
Self Discharge %/month	10	80	1	No trickkle and simple management at Launch pad
Temperature range C	0 to 40	-20 to 30	10 to 30	Management at ambient
Memory Effect	Yes	Yes	No	No reconditioning
Energy Gauge/Monitor	No	Pressure	Voltage	Better observability of State of Charge
Charge Management	CC	CC	CC CV+ Balancing	More Complex charge management
Modularity	No	No	Yes	One Cell Design, Ability to put cells in parallel

Table 5.2: Li-Ion compared to its competitors. *Source:* [66]

Table 5.3 illustrates the main characteristics of the SAFT VES180 battery:

Dimensions	53 mm x 250 mm
Specific energy	165 Wh/kg
Cell mass	1.11 kg
Energy storage	180 Wh
Mean discharge voltage	3.6 V (4.1 V at the end of charge)

Table 5.3: AFT VES180 battery specifications. *Source:* [66]

Considering a typical motor voltage of 11 V, three VES180 cells in series are needed, resulting in an assembly battery pack mass of 3.33 kg.

Finally, figure 5.5 shows the energy and capacity vs discharge current of the VES180 cell.

---

[1]The memory effect, also known as the lazy battery effect, describes the situation in which batteries gradually lose their maximum energy capacity if they are frequently charged after being partially discharged. The lack of this effect in Lithium-Ion simplifies the management of the state of charge.

[2]The Faradaic efficiency describes the electrons efficiency to be transdferred in a system facilitating an electrochemical reaction.
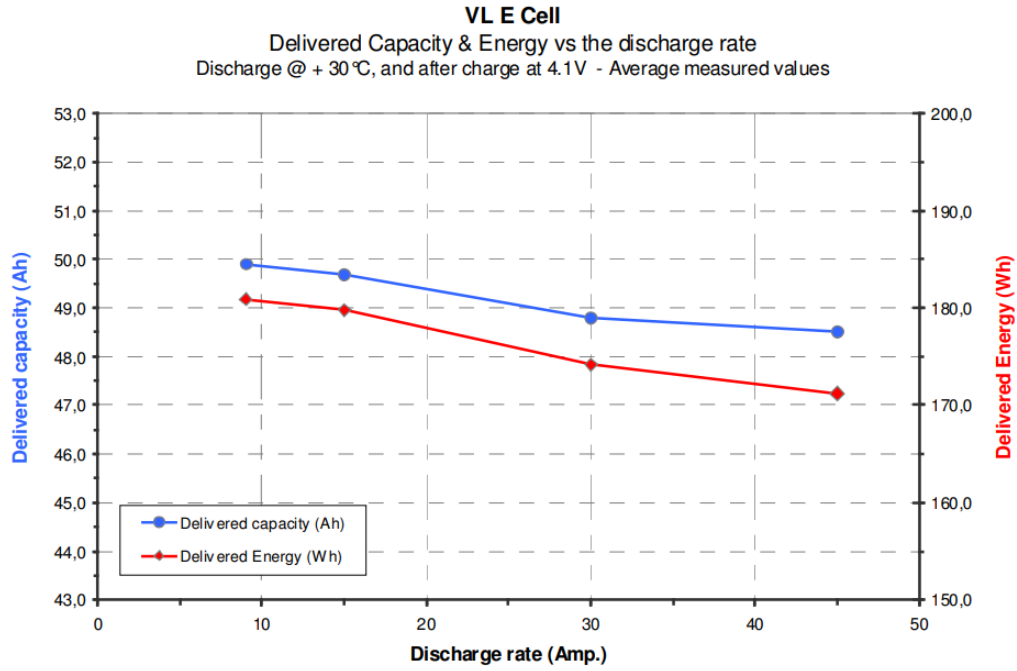
Figure 5.5: Energy and capacity vs discharge current of the VES180 cell. *Source:* [66]

Solar radiation on Mars

Solar radiation characteristics on Mars are essential to effectively design solar energy systems operating on the surface of Mars. So this subsection presents a preliminary study of solar radiation on the red planet based on [67].

The solar radiation on the surface of Mars is made from:

- The direct beam: it is the solar radiation that travels in a straight line from the Sun down to the martian surface. Its path from the top of the martian atmosphere to the surface is affected by spread and absorption.

- Diffuse component: it is the part of the total radiation that reaches the surface of Mars after a change of its directions caused by the scattering of the atmosphere.

  Furthermore, it is determined by:

  - The distance between the Sun and Mars.

  - The solar zenith angle (z).

  - The opacity of the Martian atmosphere

Thus, the direct beam irradiance (G_b) on the surface of Mars, normal to the solar rays can be calculated as:

$$G_b = G_{ob} \cdot e^{-\tau m(z)} \tag{5.7}$$

where τ is the optical depth, z is the zenith angle and m(z) is the air mass, which can be approximated by:

$$m(z) \approx \frac{1}{cos(z)} \tag{5.8}$$

Finally, the solar irradiance components on a horizontal surface of Mars are the followings (see graphics in figure 5.6):

$$G_h = G_{bh} + G_{dh} \tag{5.9}$$

where:

- G_h is the global irradiance on a horizontal surface, which is given by:

$$G_h = G_{ob} \cdot cos(z) \cdot \frac{f(z,\tau)}{0.9} \tag{5.10}$$

- G_{bh} is the direct beam irradiance on a horizontal surface, which is given by:

$$G_{bh} = G_{ob} \cdot cos(z) \, e^{\frac{-\tau}{cos(z)}} \tag{5.11}$$

- G_{dh} is the diffuse irradiance on a horizontal surface.

(a) Global irradiance. *Source:*[67]

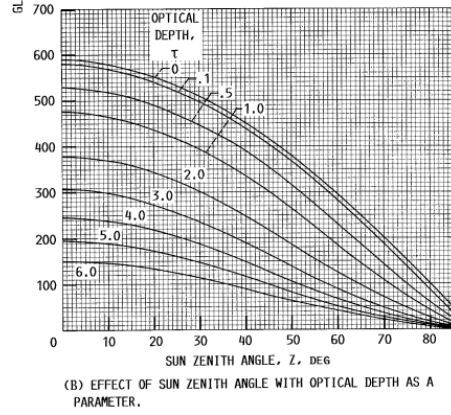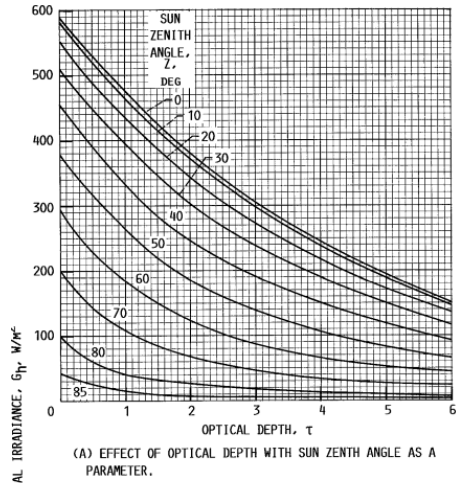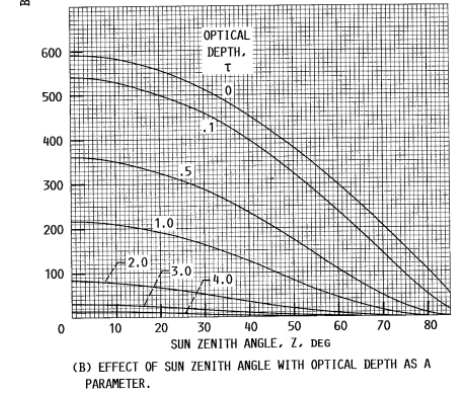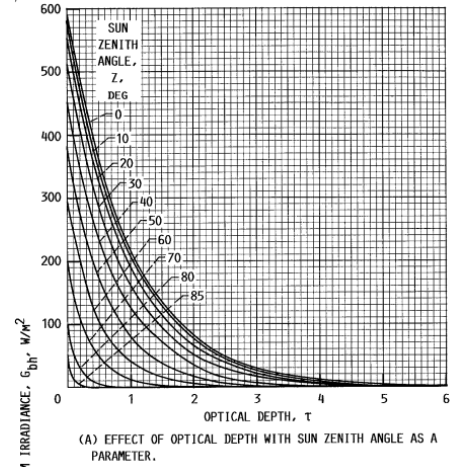(b) Direct beam irradiance. *Source:*[67]
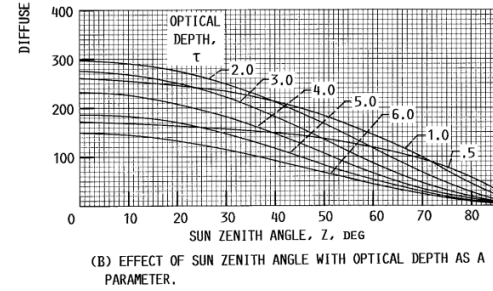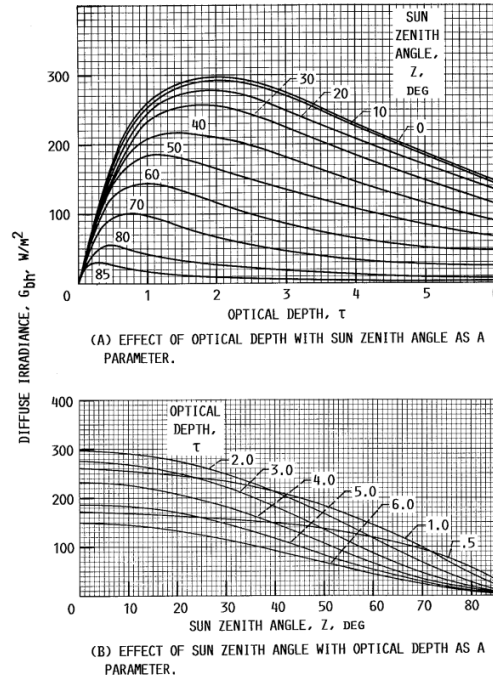
(c) Diffuse irradiance. *Source:*[67]

Figure 5.6: Solar irradiance components on a horizontal surface of Mars.

Solar panels

Space solar panels are the principal power supply in the UAV, so higher conversion efficiency, low mass power ratio and high radiation resistance are some critical challenges to consider.

Furthermore, the degradation of its electrical performance directly affects the lifetime of the mission, so researchers suggest the addition of a certain thickness of protective cover to the solar cells (such as back-surface or distributed Bragg reflector) and thinning the base layer thickness of the current-limiting subcell, or using the p-i-n structure and different doping methods for multi-junction solar cells [3] [69].

Nowadays, multijunction solar cells are one of the primary focuses for space applications due to their high efficiency and remarkable radiation resistance. Despite their high fabrication cost, they offer magnificent performance and reliable stability [69].

Figure 5.7: Ingenuity helicopter solar panel. *Source:*[68]

Thereby, the Ingenuity helicopter generates electricity through this type of solar panel, which concretely consists of high-efficiency Inverted Metamorphic Quadruple Junction cells [22].

The solar panels, which were manufactured by the SolAero company, offer high efficiency for low-irradiance low-temperature (LILT) environments. They operate at 33% efficiency (which is a remarkable result compared to the ~ 20 efficiency of regular space-grade solar panels) and they are 40% lighter than the frequently used ones [70].

Therefore, because of the arguments given below, the UAV used in the suggested mission will also generate electricity through 5 (because of the power consumption) high-efficiency Inverted Metamorphic Quadruple Junction cells (having an active area of 27.56 cm^2 each unit [70]) manufactured by SolAero Technologies:

- Lower-cost compared to radioisotope thermoelectric generators.

- High reliability.

- Higher efficiency compared to the regular space-grade solar panels.

- More power per unit area than the current SoP at LILT.

---

[3]Multi-junction solar cells are multiple p-n junctions made of different semiconductor materials, whiches improve the energy conversion efficiency by allowing the absorbance of a wider range of wavelengths (see figure 5.8).
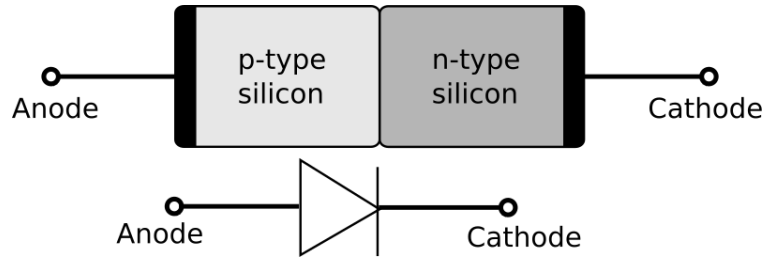
Figure 5.8: A p–n junction. *Source:*[71]

5.1.6 Thermal Subsystem

The Thermal Subsystem plays a crucial role in the optimal performance and maintenance of the UAV. Its design not only shall minimize survival heater energy but also maintain acceptable flight temperatures by absorbing enough solar energy on the exterior of the fuselage during the daytime and minimizing heat loss at night. Therefore, the design selected is based on the one used for the Ingenuity helicopter [72], as it has been carefully studied and successfully tested.

Considering the cold environment of Mars, the fuselage shall protect the elements that it hosts: the avionics processing, instruments, sensors and batteries. Hence, it is proposed a Kapton dark film material as a fuselage outer layer because of its properties:

- High thermal absorptivity in the daytime.

- Low emissivity at night, when the battery survival heater is required.

The sporadically Martian dust storms also have to be taken into consideration due to the tendency to bias the solar absorptivity of the surface material while relatively unaffect the infrared emissivity. Nevertheless, the dust is predicted to have a minimal impact on the absorptivity of the fuselage and be removed when the UAV flies.

Finally, some heaters shall keep the batteries warm at night. Moreover, these batteries are insulated to conserve energy by using low thermal conductivity materials and CO_2 gas gaps [4].

---

[4]The CO_2 gas gaps are large enough gaps between components that are open to the Mars atmosphere in order to take advantage of conductive isolation without being too large to introduce convection.

5.1.7 Landing Subsystem

This subsection is divided into 2 different parts: the selection of the landing gear configuration and the emergency parachute of the UAV.

Landing gear

The election of the landing gear is based on the comparison of the 3 configurations shown in figure 5.9:

(a) Ingenuity helicopter landing gear. *Source:* [73]

(b) Dragonfly landing gear. *Source:* [74]

(c) The Martian Autonomous Rotary-wing Vehicle (MARV). *Source:* [75]
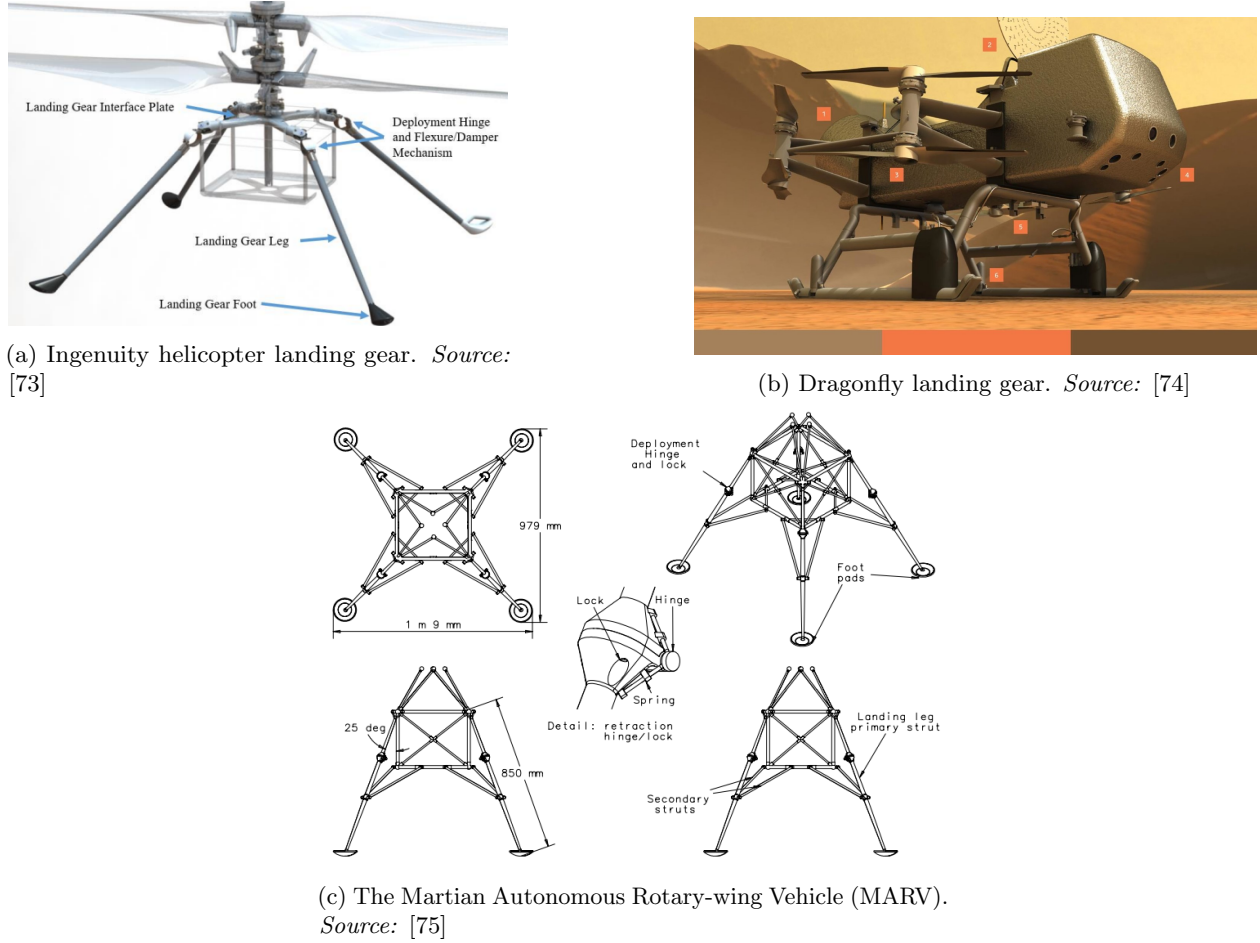
Figure 5.9: 3 possible landing gear configurations for the Martian UAV

- **Ingenuity helicopter landing gear:** it is designed to accommodate extensive dynamic landing conditions and surface features. The large footprint provides a stable base and reduces the risk of tip-over, and the material used to build the legs, TeXtreme ®(see section 5.1.9 for further information), contributes to making a more rigid and lightweight landing gear structure. As figure 5.9a illustrates, the four landing gear legs are attached to a composite plate bonded to the mast of the helicopter and the latching deployment hinges at the top of the landing gear allow its folding to accommodate the helicopter into the rover's belly. Furthermore, a titanium flexure with a yielding 1100-series aluminum damper conducts suspension tasks to buffer the landing [73].

- **Dragonfly landing gear:** unlike Ingenuity, the Dragonfly is still under design. Specifically, its subsystems and instruments were subjected to review in July and August 2022 and the APL has also begun testing flights with a half-scale octocopter at California's Imperial Dunes, Arizona. However, the proposed landing gear configuration is still taken into consideration because of its simplicity and the difference between the two other configurations. As figure 5.9b illustrates, the landing gear consists of two landing skids equipped with 2 wheels at the front. The landing legs, as structural attachments, are designed to minimize the heat leak from the lander interior to the external environment and its landing struts contain the shock-absorbing mechanism [74, 23].

- **The Martian Autonomous Rotary-wing Vehicle (MARV) landing gear:** it consists of four simple and lightweight legs that end with an articulated food pad made of crushable aluminum honeycomb (which avoids the tendency to bounce) and allows the vehicle to adapt to slopes and rocks. The saucerlike shape design decreases stress on impact and avoids instability on touchdown and the overall landing gear can absorb different impact loads [75].

Concisely, the arguments listed below justify the landing gear choice for this bachelor's final thesis, the one used in the Ingenuity helicopter:

- The UAV is not expected to require movement when not flying, so the wheels of the Dragonfly concept are not required. Moreover, they would increase the weight of the vehicle and the rough Martian terrain conditions wouldn't ease the wheeled movement. Consequently, the Dragonfly landing gear concept is rejected.

- The Ingenuity helicopter design has been widely tested, even on the Mars surface during the successful > 30 flights of the vehicle. Moreover, its large footprint provides major stability, it has a simple design and it is made of a material that has demonstrated a reliable and satisfactory performance.

Emergency parachute

Although the coaxial design of the UAV prevents the vehicle from various issues that can occur, it has been considered the insertion of an emergency parachute in the multirotor preliminary design to protect the different instrumentation and recover data in case of failure.

The choice would consist of a COTS model, the $6,0\ m^2$ (8kg Multirotor) - Opale drone rescue parachute (see figure 5.10), if the UAV was designed to fly on Earth because of its compatibility within different UAVs, compaction, lightness ($350\ g$ without the mass of the required servo), robustness and rapidity to unfold on the order of a split second to ensure a soft landing and is equipped with reinforcements [76].

Figure 5.10: Opale drone rescue parachute. *Source:* [76]

However, Earth parachutes don't work on Mars because the atmospheric density of the red planet is much lower than on Earth, resulting in the inability of the parachute chosen to slow down the UAV in case of an emergency.

Thus, the selection of the appropriate parachute for the UAV is based on [77].

The type configuration of the parachute will be chosen within the slotted textile parachutes group for their characteristics:

- They are the most common parachute type used in planetary exploration missions.

- They have extensive openings through the canopy in addition to the vent (see figure 5.11 for parachute terminology).

- They are fabricated from cloth materials or ribbons.

- They provide better drag-stability trade space.

Nevertheless, they can be expensive to manufacture.
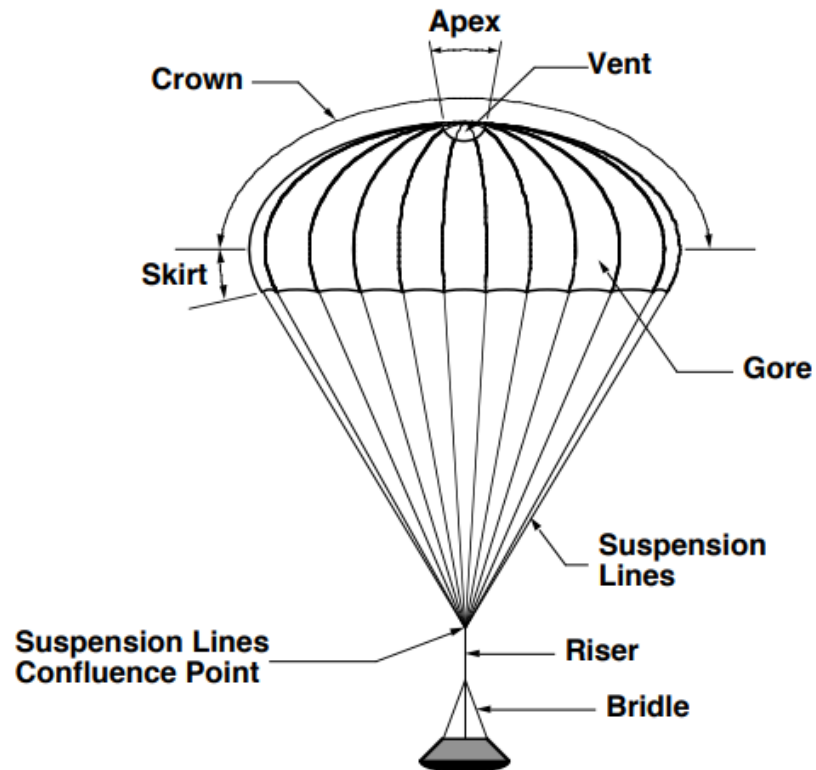
Figure 5.11: Parachute terminology. *Source:* [77]

From the shape configurations shown in figure 5.12, 4 types of canopies are widely used for planetary exploration missions (see the list below), so one of them will be the chosen configuration shape for the emergency parachute of the UAV.

- Guide Surface.

- Conical Ribbon.

- Disk-Gap-Band (solid textile parachute).

- Ringsail.

The Disk-Gap-Band and the Conical Ribbon parachutes are dismissed because they have a relatively high weight per unit area. So the Ringsail parachute (see figure 5.12 for its parameters and general application) is chosen because:

- It produces high drag ($C_{D0} \sim 0.8$) with good-to-moderate stability ($\pm 5°$to $\pm 10°$ average angle oscilation).

- It is relatively light weight per unit area.

- Its design is tailored for optimum performance by varying the canopy shape and the distribution of the geometric porosity throughout the canopy.
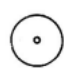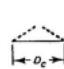
Type	Constructed Shape		$\dfrac{D_c}{D_o}$	Inflated Shape $\dfrac{D_p}{D_o}$	Drag Coef. C_{D_o} Range	Opening Load Factor C_X (Inf. Mass)	Average Angle of Oscillation	General Application
	Plan	Profile						
Flat Ribbon			1.00	.67	.45 to .50	~1.05	0° to ±3°	Drogue, Descent, Deceleration
Conical Ribbon			.95 to .97	.70	.50 to .55	~1.05	0° to ±3°	Descent, Deceleration
Conical Ribbon (Varied Porosity)			.97	.70	.55 to .65	1.05 to 1.30	0° to ±3°	Drogue, Descent, Deceleration
Ribbon (Hemisflo)			.62	.62	.30* to .46	1.00 to 1.30	±2°	Supersonic Drogue
Ringslot			1.00	.67 to .70	.56 to .65	~1.05	0° to ±5°	Extraction, Deceleration
Ringsail			1.16	.69	.75 to .90	~1.10	±5° to ±10°	Descent
Disc-Gap-Band			.73	.65	.52 to .58	~1.30	±10° to ±15°	Descent

Figure 5.12: Types and functions of slotted textile parachutes. *Source:* [78]

5.1.8 Communications Subsystem

The Communications Subsystem allows the exchange of information (data transmission and reception) between the swarm of UAVs and the swarm of rovers, which consists of an antenna and a chipset. Specifically, an omnidirectional antenna, assembled on top of the solar panel, allows communication between the UAVs and the rovers and the radio link to ensure the communication is implemented by a chipset mounted in the vehicles of both swarms that uses the low-power Zigbee communication protocols [5] [22, 40, 81, 82].

5.1.9 Structural Subsystem

This subsection is divided into 2 different parts: the selection of the fuselage materials of the UAV and the deployment mechanism of tit on the Martian surface.

Materials selection

The selection of the fuselage materials of the UAV is based on the materials used to build the Ingenuity helicopter, as they have been tested to resist the harsh environment of Mars [20, 22, 64].

Accordingly, the materials that define the structure of the UAV shall be solid enough to withstand the Martian rough conditions. From one hand, the cooler temperatures of the planet and its variation is one of the obstacles that has to be deeply taken into account when designing the UAV. From the other hand, the dry and practically oxygen-free atmosphere of Mars [6] results in one advantage: materials are not corroded. Furthermore, for designing aerospace vehicles, weight and high strength/weight and stifness/weight ratios are relevant, which include metallic alloys, such as aluminium and titanium alloys, and different composite materials [75].

Therefore, the material used for the blades, the landing legs, the solar panel substrate and the fuselage is TeXtreme ®, a new intertwined carbon fiber called **Spread Tow**, which consists of using some kind of strips instead of the commonly used threads. This fiber architecture not only provides better conditions for reducing weight and optimizing the laminate thickness but also suppresses microcracking and avoids or counteracts the subsequent effects of composite failure, which leads to longer-lasting parts [83, 84].

Deployment mechanism

As section 4.3.2 indicates, it is not necessary to fold the UAVs to introduce theminside the lander. Consequently, any additional deployment mechanism is required, which simplifies the design of the UAV.

---

[5]Zigbee is an open, standard, secure and reliable wireless communication technology standard between wireless devices used with small, low-power, low-data rate digital radios, such as lightweight UAVs [79, 80].

[6]The atmosphere of Mars consists of 95.32% of carbon dioxide, 0.13% oxygen, 0.03% water and small concentrations of other elements.

5.1.10   OBC Subsystem

The Onboard Computer (OBC) Subsystem provides processing capability to the UAV. Thus, it is the software that implements the vital functions of the drone, which are listed below with others:

- Attitude and control.

- Execution or transmission telecommands.

- Failure detection.

- Isolation and recovery.

- On Board time management.

- Autonomous Reconfiguration.

- Local Mass Memory function.

- Cleaning telemetry to monitor the health and functioning of the UAV.

- Interfacing with other subsystems.

Because of its need to interface with other subsystems in order to acquire data to perform its duties, this processor requires a piece of hardware that consists of a microprocessor, memory banks and an interfacing chip to connect the computer to different abroad sensors and actuators [85].

There are a wide variety of OBC softwares in the market. However, this bachelor's final thesis considers the F' Flight Software & Embedded Systems Framework [86], an open-source multi-mission [7] flight software created at NASA's JPL, because of its reliability and reusability [87].

It was created to streamline and decrease the software development cost to allow the easy reusing of written components from one application to another while having the ability to be run on a wide range of processors. Furthermore, it has been successfully tested abroad the International Space Station (ISS)-RapidScat scatterometer instrument [8] [88], the JPL's ASTERIA CubeSat [9] [89] and the Ingenuity helicopter.

---

[7]The F' Flight Software & Embedded Systems Framework was designed for CubeSats, small spacecraft and instruments.
[8]The International Space Station (ISS)-RapidScat scatterometer instrument monitored ocean winds to provide essential measurements for weather predictions, including hurricane monitoring.
[9]The ASTERIA CubeSat was designed to study planets outside the Solar System.

5.1.11 Mass distribution diagram

As the overall mass of the UAV is estimated to be around ∼8 kg, it is considered to present the mass distribution diagram shown in figure 5.13, which proportion is based on [40]:
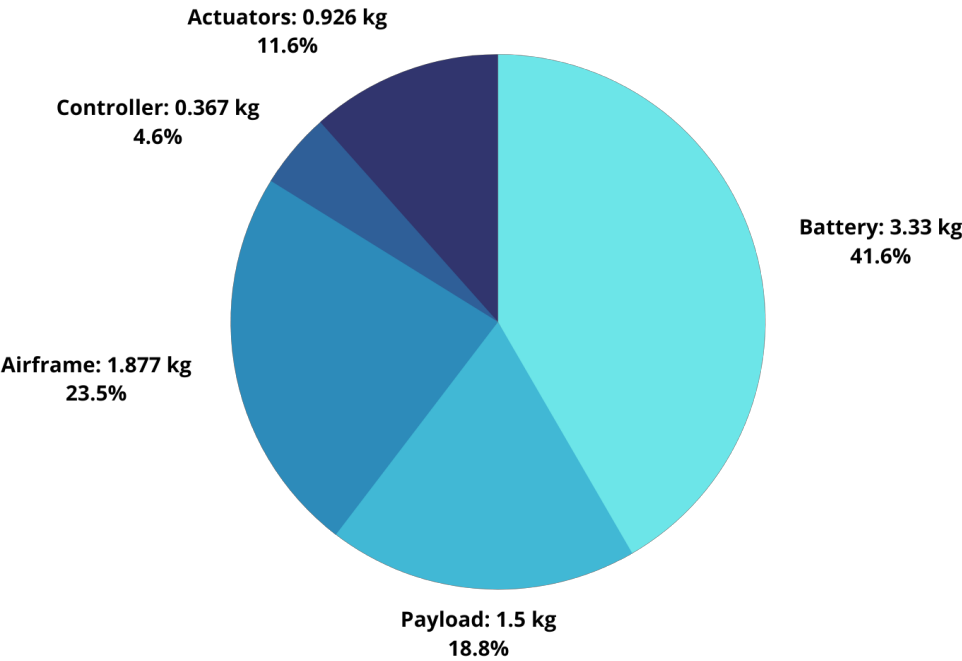
Figure 5.13: Mass distribution diagram *Source:* own elaboration

Chapter 6

The swarm of UAVs

6.1 Swarm overview

Over the last years, there has been a development of the control theory and artificial intelligence, which has led to deep research in the multi-agent formation control field. Studies that emphasize the potential problem of formation controlling (like the work of Baillieul and Suri [90]), which goal consists of driving a group of mobile autonomous agents in a desired shape, have increased the focus on the field and delved into deeper investigations.

It has been demonstrated in many applications (such as exploration or research) [91, 92] that coordinating robotic agents to cooperatively execute a task is more advantageous and successful when maneuvering them in a group formation.

Hence, formation control problems are divided into two categories according to variables: position-based and distance-based. In distance-based formation control, control law is always nonlinear, independently of agent models, which increases the complexity of the analysis of the stability of the multi-agent system. In contrast, the position-based formation, with a common leader, turns out to be simpler and converges exponentially fast to a desired shape formation from any initially non-collinear position [92].

This bachelor's final thesis considers a triangular formation formation (which is developed in depth in section 6.3) because it is the simplest formation that considers asymmetric co-leader relation and it is rigid. [93, 92]. Thus, three UAVs are considered for the suggested mission, each of them locally controlling its own position so that the distance to the next agent (its co-leader) remains constant.
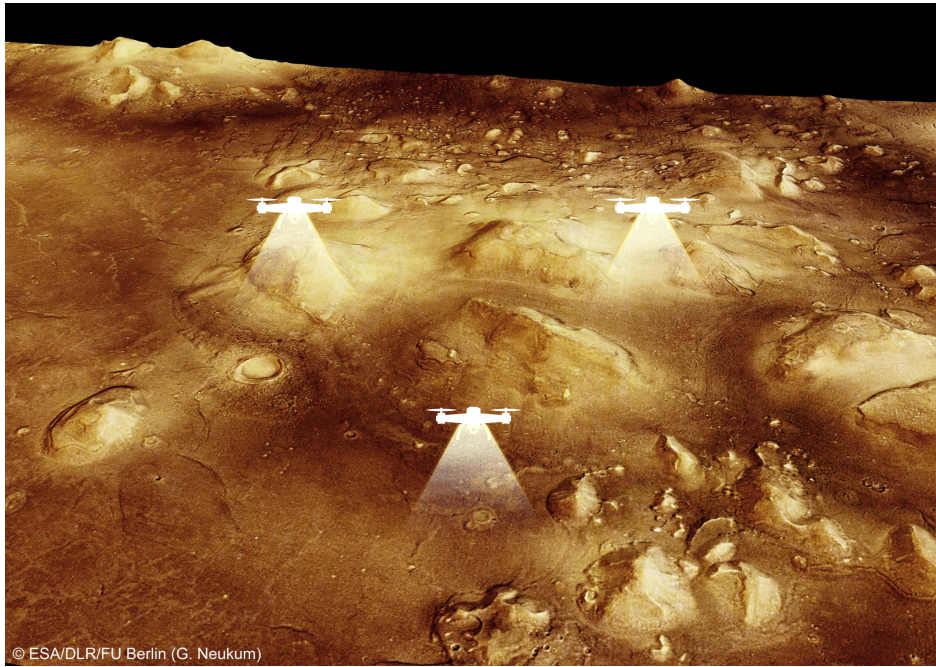
Figure 6.1: Concept illustration of the swarm of UAVs on Cydonia Mensae. *Source: own elaboration based on* [94]

6.2 Pre-flight check procedures

Before the formation flight of the swarm, it is fundamental to ensure the appropriate performance of the sensors of the ACDS. Hence, although the OBC Subsystem is responsible for providing the processing capabilities of the UAVs, it has been considered the approach of simplified algorithms (whiches can be consulted in the appendices) formulated in the Arduino programming language[95], which has been introduced in an optional subject of the concentration itinerary in UAVs.

An Arduino sketch is divided into 3 main parts:

1. Variable declaration section.

2. Setup section: it collects the configuration information, which consists of the initialization data of the elements, and it is only executed once.

3. Loop section: it contains the cyclically executed program.

6.2.1   IMU

Orientation of the accelerometer

This program reads the accelerometer data and translates it to orientation. In order to achieve that, a COTS miniature sensor is selected to do the test [96].

Algorithm 1: Orientation of the accelerometer.

Inclusion of external libraries :	CurieIMU.h
Variable declaration section :	introduction of the previous orientation (for comparison);
Setup :	definition of the default speed for the serial monitor and data print to the serial port, wait for the serial port to open, initializing the IMU device and set the accelerometer range;
Loop :	defining the orientation of the board and the printing description of the orientation, reading the accelerometer data, calculating the absolute values of each axis and printing the changes in orientation;

Reading data of the accelerometer

This program reads the accelerometer. In order to achieve that, a COTS miniature sensor is selected to do the test.

Algorithm 2: Orientation of the accelerometer.

Inclusion of external libraries :	CurieIMU.h
Variable declaration section; :	-
Setup :	definition of the default speed for the serial monitor, wait for the serial port to open, initializing the IMU device and set the accelerometer range;
Loop :	defining the scaled accelerometer values, reading and displaying the accelerometer measurements;

6.2.2 Inclinometer

This section suggests two algorithms [97]: a self-test and the assurance of reading the roll and pitch angles.

Self-test algorithm

This program puts the device in self-test mode and reads the test results. In order to achieve that, a COTS miniature sensor is selected to do the test.

Algorithm 3: Self test of the inclinometer.

Inclusion of external libraries	: SCA100T.h
Variable declaration section	: pin selection, selection of the maximum data transfer speed and selection of the type of sensor;
Setup	: definition of the default speed for the serial monitor and data print to the serial port *(the introduction of F() allows moving constant strings to the program memory instead of the RAM)*;
Loop	: self-test on the X-axis, self-test on the Y-axis and impression of the read values;

Reading of the roll and pitch angles algorithm

This program reads the X and Y angles (roll and pitch) from the sensor and prints them to a serial port. In order to achieve that, a COTS miniature sensor is selected to do the test.

Algorithm 4: Reading and impression of the roll and pitch angles of the inclinometer.

Inclusion of external libraries	: SCA100T.h
Variable declaration section	: pin selection, selection of the maximum data transfer speed and selection of the type of sensor;
Setup	: definition of the default speed for the serial monitor and data print to the serial port *(the introduction of F() allows moving constant strings to the program memory instead of the RAM)*;
Loop	: getting and printing the X and Y angles;

6.2.3 LiDAR

This section suggests an algorithm that consists of the initialization, configuration and reading of the distance from a selcted COTS LiDAR sensor [98]

Algorithm 5: Reading and impression of the roll and pitch angles of the inclinometer.

Inclusion of external libraries : Wire.h and LIDARLite.h	
Variable declaration section	: declaration of the LiDAR sensor;
Setup	: definition of the default speed for the serial monitor and data print to the serial port and set the configuration to default;
Loop	: measure with receiver bias correction and print to the serial terminal;

6.3 Triangular Formation Algorithm

The Triangular Formation Algorithm (TFA) [92, 93, 99, 100, 101] is a scalable and practical mechanism resulting in swarm behaviors as the basic requirements for implementing it on a UAV are minimal.

As it is based on local interaction between UAVs, its primary objective is to make three neighboring UAVs form a dynamic triangular mesh-based formation, regardless of their initial positions. Concretely, the formed triangle is isosceles.

Furthermore, there is no need for synchronization or communication between the UAVs except for sharing their current state, and the constant distance ($\bar{d}$) between the vehicles is a predefined parameter (equal to the side length of the triangle) chosen according to the prescribed minimum safety distance between UAVs ($\bar{d} > d_{safety}$). Hence, each agent of the swarm locally controls its own position.

The basic structure of the algorithm requires the UAVs to perform only three local behaviors and execute them periodically. These local behaviors are:

1. Detecting the position of the other UAVs.

2. At each discrete time-step, the i-th UAV calculates the desired position $\hat{P}_i = [\hat{x}_i(t), \hat{y}_i(t)]^T$, which forms an isosceles triangle with the other two neighbors.

3. Moving towards the goal position.

Thus, considering the position of the i-th UAV $P_i(t)$ and its two neighbors in the swarm, whose positions are $P_j(t)$ and $P_k(t)$ respectively, the position $P_k(t)$ of the k-th UAV has to be placed symmetrically to $P_j(t)$:

$$P_k(t) = [\, x_i(t) - \mid P_i(t) - P_j(t) \mid sin\psi_i(t), \; y_i(t) + \mid P_i(t) - P_j(t) \mid cos\psi_i(t)\,] \qquad (6.1)$$

where $\mid P_i(t) - P_j(t) \mid$ is the distance between the i-th and j-th UAVs and ψ_i is the heading of the i-th UAV.

Then, assuming that $\mid P_i(t) - P_j(t) \mid \leq \mid P_i(t) - P_k(t) \mid$ and $\mid P_j(t) - P_k(t) \mid \leq 2\bar{d}$ the desired position $\hat{P}_i = [\hat{x}_i(t), \hat{y}_i(t)]$ can be calculated as:

$$\begin{cases} \hat{x}_i(t) = x_M(t) - h \cdot sin\theta_{jk}(t) \\ \hat{y}_i(t) = x_M(t) + h \cdot cos\theta_{jk}(t) \end{cases} \quad if \; 0 \; \leq \; \Delta\theta(t) < \pi \tag{6.2}$$

$$\begin{cases} \hat{x}_i(t) = x_M(t) + h \cdot sin\theta_{jk}(t) \\ \hat{y}_i(t) = x_M(t) - h \cdot cos\theta_{jk}(t) \end{cases} \quad if \; \pi \; \leq \; \Delta\theta(t) < 2\pi \tag{6.3}$$

where:

- $P_M(t)$ is the mean point between $P_j(t)$ and $P_k(t)$:

$$P_M(t) \; = \; \frac{P_k(t) \; + \; P_j(t)}{2} \; = \; (x_M(t), y_M(t))^T$$

- h is the height of the triangle:

$$h \; = \; \sqrt{\bar{d}^2 \; - \; \mid P_M(t) \; - \; P_j(t) \mid^2}$$

- $\Delta\theta$ is the angle increase:

$$\Delta\theta \; = \; \lfloor \theta_{jk}(t) \; - \; \theta_{iM}(t) \rfloor_0^{2\pi}$$

whith:

$$\theta_{jk}(t) \; = \; \lfloor atan2(y_j(t) \; - \; y_k(t), \; x_j(t) \; - \; x_k(t)) \rfloor_0^{2\pi}$$

$$\theta_{iM}(t) \; = \; \lfloor atan2(y_M(t) \; - \; y_i(t), \; x_M(t) \; - \; x_i(t)) \rfloor_0^{2\pi}$$

where atan2 (α) represents the 2-argument of the arctangent function, and the operator $\lfloor \alpha \rfloor_0^{2\pi}$ wraps the angles in the range $[0, 2\pi]$.

According to equations 6.2 and 6.3, the resulting isosceles triangle formed by $\boldsymbol{P_j \hat{P}_i P_k}$ is illustrated in figure 6.2:
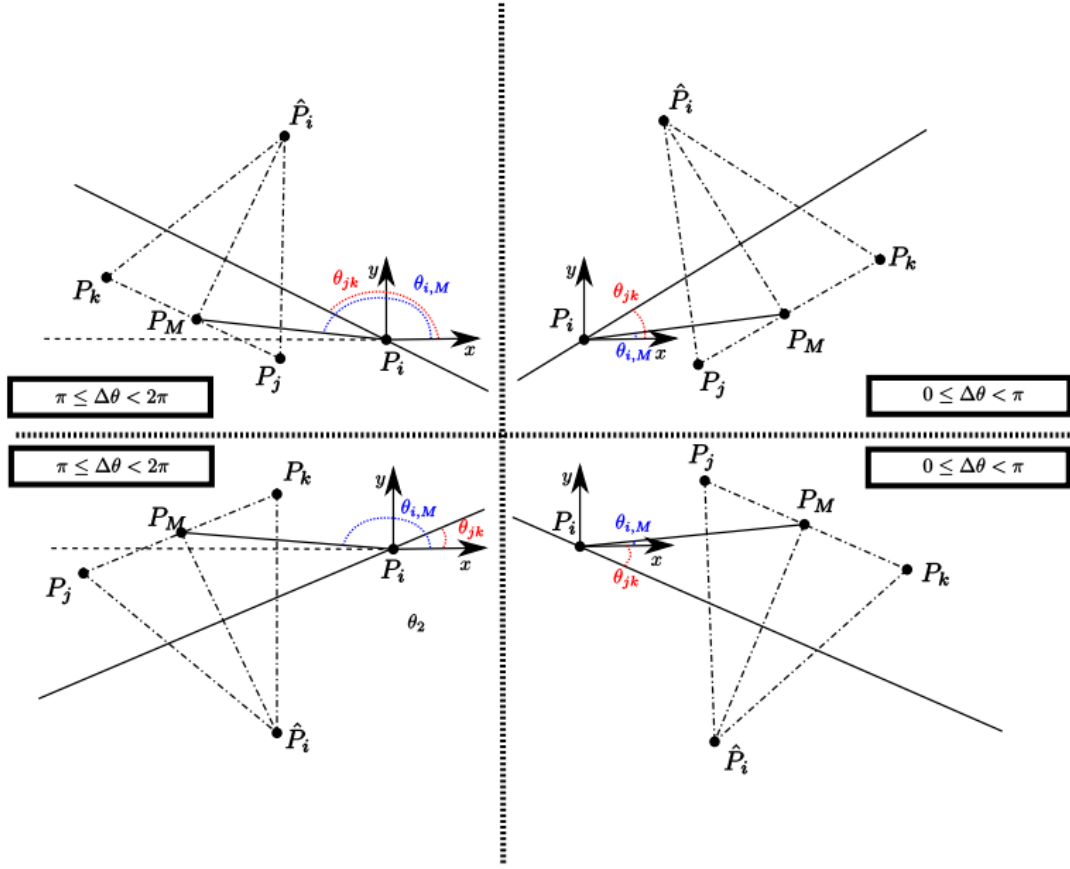
Figure 6.2: TFA isosceles triangle construction cases. Time information has been omitted. *Source:* [99]

Figure 6.2 shows the 4 TFA construction cases in accordance with the initially non-collinear positive or negative orientation of the UAVs.

Moreover, another consideration has to be taken into account: if the length of one of the edges of the resulting triangle is greater than twice the desired distance between the UAVs, the UAVs have to be approached, so the desired position $\hat{P}_i(t)$ has to be computed as:

$$\hat{P}_i(t) \;=\; \frac{P_i(t) \;+\; P_j(t) \;+\; P_k(t)}{3} \tag{6.4}$$

Finally, following the calculations and information given above, and omitting the time information, the TFA procedure algorithm is summarized in algorithm 6.

Algorithm 6: Triangular Formation Algorithm.

Data: P_i, P_j, P_k

Parameter: $\bar{d}$

Result: $\hat{P}_i$

if $\bar{d} < \frac{P_j \bar{P}_k}{2} \vee \bar{d} < \frac{P_i \bar{P}_k}{2} \vee \bar{d} < \frac{P_i \bar{P}_j}{2}$ **then**

$\quad \left| \quad \hat{P}_i = \frac{P_i + P_j + P_k}{3};$

else

$\quad \left| \quad P_M = \frac{P_j + P_k}{2};$

$\quad \quad \theta_{jk} = \lfloor atan2(y_j - y_k, \ x_j - x_k)\rfloor_0^{2\pi};$

$\quad \quad \theta_{i,Mk} = \lfloor atan2(y_M - y_i, \ _xM - x_i)\rfloor_0^{2\pi};$

$\quad \quad \Delta\theta = \lfloor \theta_{jk} - \theta_{i,Mk}\rfloor_0^{2\pi};$

$\quad \quad h = \sqrt{\bar{d}^2 - \mid P_M - P_j \mid^2};$

$\quad \quad$ **if** $0 \leq \Delta\theta < \pi$ **then**

$\quad \quad \left| \quad \hat{P}_i = (x_M - h \cdot sin\theta_{jk}, \ y_M + h \cdot cos\theta_{jk});$

$\quad \quad$ **else**

$\quad \quad \left| \quad \hat{P}_i = (x_M + h \cdot sin\theta_{jk}, \ y_M - h \cdot cos\theta_{jk});$

$\quad \quad$ **end**

end

Firstly, figure 6.3 validates that the initial positions of the j-th and k-th UAVs are symmetric, which is an essential step to construct the isosceles triangle.
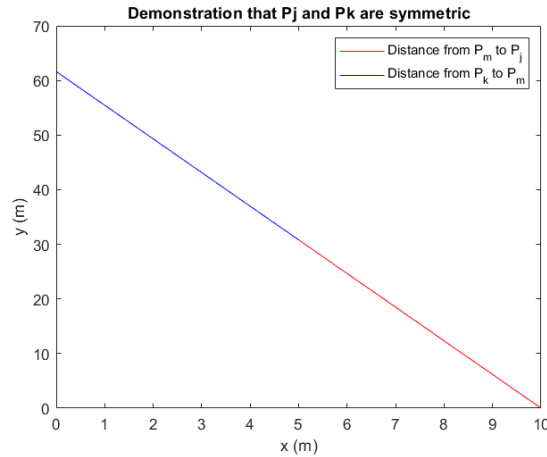
Figure 6.3: Verifying that Pk and Pj are symmetric. *Source: own elaboration*

Secondly, figure 6.4 presents 4 different initial cases to demonstrate that the isosceles triangle can be constructed regardless of the initial positions of the i-th and j-th UAVs.
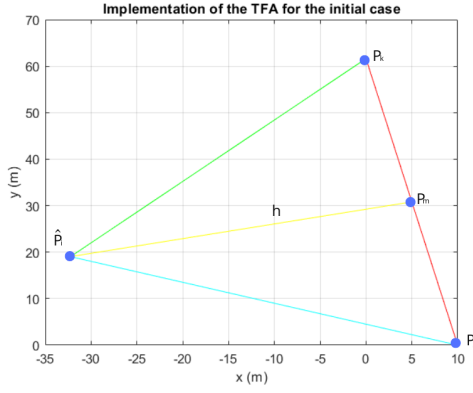
(a) Implementation of the TFA for the initial case 1.
Source: own elaboration
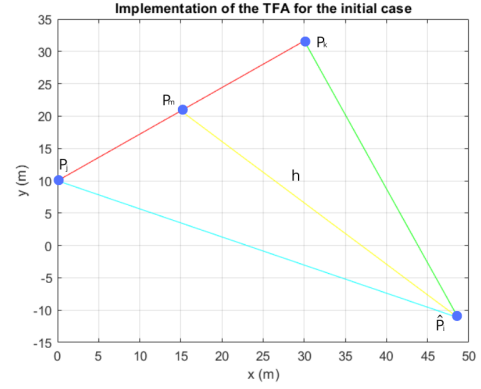
(b) Implementation of the TFA for the initial case 2.
Source: own elaboration
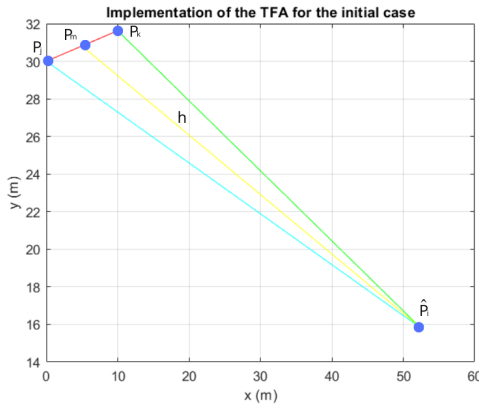
(c) Implementation of the TFA for the initial case 3.
Source: own elaboration
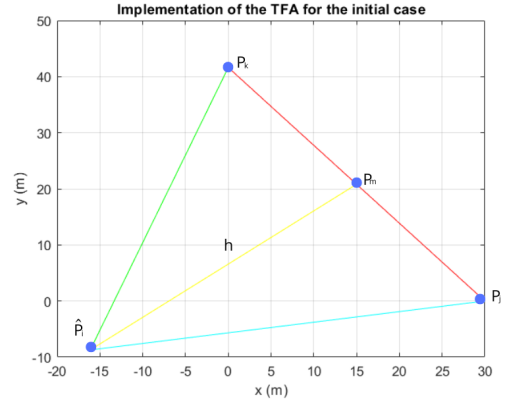
(d) Implementation of the TFA for the initial case 4.
Source: own elaboration

Figure 6.4: Implementation of the TFA for 4 initial cases. *Source: own elaboration*
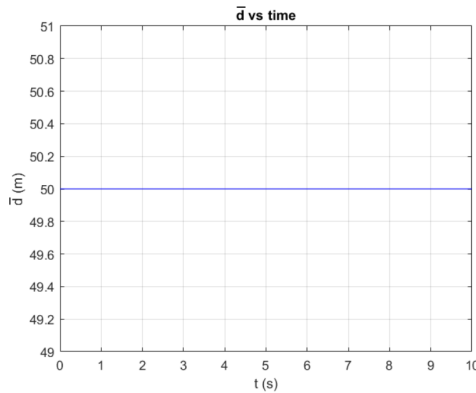
(a) Demonstration of the time independence of $\hat{d}$.
Source: own elaboration
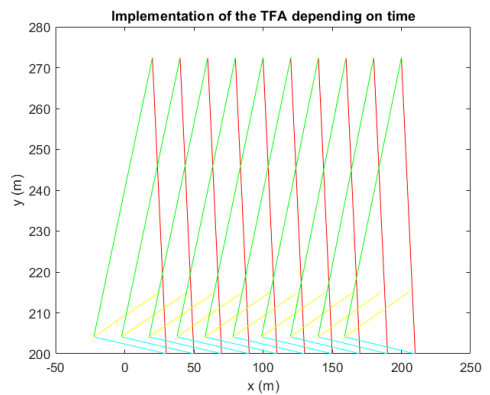
(b) Implementation of the TFA depending on time.
Source: own elaboration

Figure 6.5: Demonstration of the time independence of $\hat{d}$ and implementation of the TFA depending on time.
Source: own elaboration

Afterwards, the TFA is applied without omitting the time information. Figure 6.5a verifies that $\hat{d}$ is a predefined constant parameter related to the distance between the UAVs which satisfies the condition: $\bar{d} > d_{safety}$. Besides, figure 6.5b illustrates and validates the implementation of the TFA in a period of time.

So, the next step suggested for the swarm of UAVs is shown in section 6.4.

6.4   Leader - follower formation keep

The formation flight control strategy of a swarm of UAVs usually includes formation flight control based on behavior, a leader-follower pattern formation flight control and formation flight control based on virtual structure. Considering that the first one was already applied in the TFA section and that the leader-follower pattern formation flight control can be affected by a large amount of interference because the formation strategy is based on preset formation structure, this section is focused on the formation flight control based on virtual structure suggested in [102]. This method adopts a virtual structure, which allows the avoidance of interference.

The formation geometry of the leader and one of the followers is shown in figure 6.6.
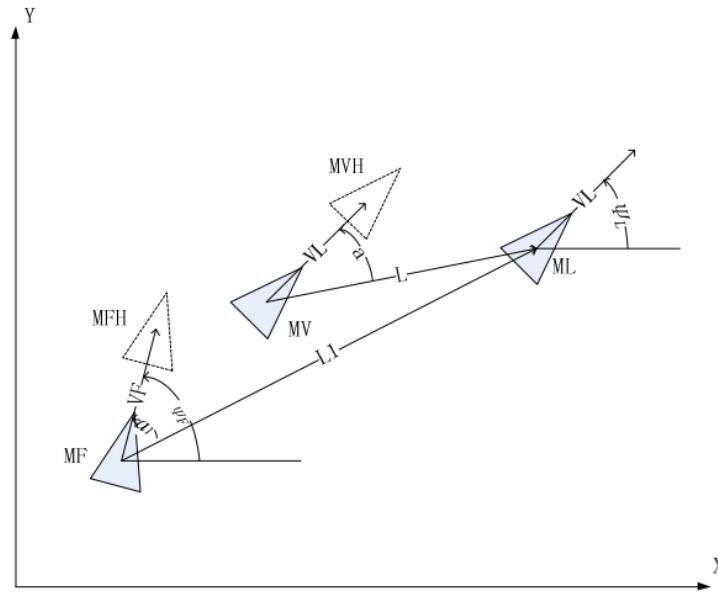
Figure 6.6: Formation geometry of the leafer and one follower. *Source:* [102]

Where:

- The X-axis represents the est.

- The Y-axis represents the north.

- ML is the UAV leader of the formation.

- MF is one of the UAV followers.

- MV is the follower set by virtual structure.

- MFH represents the position of MF in the interval of δt (which is the communication network delay).

- MVH represents the position of MV in the interval of δt

- VF represents the horizontal distance between MFH and MF.

- VL represents the horizontal distance between MVH and MV.

- ψ_L is the trajectory yaw angle of ML.

- ψ_F is the trajectory yaw angle of MF.

- l is the displacement in the communication cycle of ML and MF.

Establishing the UAVs of the swarm in a state of constant altitude flight control, the relationship between ML and MVH can be expressed as:

$$
\begin{cases}
x_{MVH} = x_{ML} - L \cdot cos(\psi_L - a) + l \cdot cos\psi_L \\
y_{MVH} = y_{ML} - L \cdot sin(\psi_L - a) + l \cdot sin\psi_L
\end{cases}
\tag{6.5}
$$

where x_{MVH}, y_{MVH}, x_{ML} and y_{ML} represent the east and north position of MVH and ML, L represents the excepted distance from MVH to ML and and a represents the observation angle from MVH to ML.

On the other side, the relationship between MF and MFH:

$$
\begin{cases}
x_{MFH} = x_{MF} + l \cdot cos\psi_F \\
y_{MFH} = y_{MF} + l \cdot sin\psi_F
\end{cases}
\tag{6.6}
$$

where x_{MFH}, y_{MFH}, x_{MF} and y_{MF} represent the east and north position of MFH and MF.

From equations 6.5 and 6.6, the tracking error between MVH and MFH is:

$$
\begin{cases}
e_x = x_{MFH} - x_{MVH} = x_{MF} + l \cdot cos\psi_F - x_{ML} - L \cdot cos(\psi_L - a) + l \cdot cos\psi_L \\
e_y = y_{MFH} - y_{MVH} = y_{MF} + l \cdot sin\psi_F - y_{ML} - L \cdot sin(\psi_L - a) + l \cdot sin\psi_L
\end{cases}
\tag{6.7}
$$

Differentiating equation 6.7:

$$
\begin{cases}
\dot{e_x} = V_F \cdot cos\psi_F - l\omega_F \cdot sin\psi_F - V_L \cdot cos\psi_L - L\omega_L \cdot sin(\psi_L - a) + l\omega_L \cdot sin\psi_L \\
\dot{e_y} = V_F \cdot sin\psi_F - l\omega_F \cdot cos\psi_F - V_L \cdot sin\psi_L - L\omega_L \cdot sin(\psi_L - a) + l\omega_L \cdot cos\psi_L
\end{cases}
\tag{6.8}
$$

V_L and V_F represent the velocity of ML and MF, while ω_L and ω_F represent the yaw rate of ML and MF.

Applying a coordinate transformation, the errors e_x and e_y are transfered to the coordinate of velocity of MF:

$$
\begin{cases}
\bar{e_x} = e_x \cdot cos\psi_F + e_y \cdot sin\psi_F \\
\bar{e_y} = -e_y \cdot sin\psi_F + e_y \cdot cos\psi_F
\end{cases}
\tag{6.9}
$$

Differentiating equation 6.9 and combining it with equations 6.7 and 6.8:

$$\begin{cases} \dot{\bar{e}}_x = V_F - V_L \cdot cos(\psi_L - \psi_F) - L\omega_L sin(\psi_L - \psi_F - a) + l\omega_L sin(\psi_L - \psi_F) + \omega_F \bar{e}_y \\ \dot{\bar{e}}_y = l\omega_F - V_L \cdot sin(\psi_L - \psi_F) + L\omega_L cos(\psi_L - \psi_F - a) - l\omega_L cos(\psi_L - \psi_F) - \omega_F \bar{e}_y \end{cases} \quad (6.10)$$

Considering the Lyapunov function, which is used to prove the stability of an equilibrium of an ODE:

$$\begin{cases} V = \bar{e_x}^2 + \bar{e_y}^2 \\ \dot{V} = 2\bar{e_x}\dot{e_x} + 2\bar{e_y}\dot{e_y} \end{cases} \quad (6.11)$$

and according to the Lyapunov law, for a given error $(\bar{e_x}, \bar{e_y}) \neq$ the error of $\bar{e_x}$ and $\bar{e_y}$ can converge to zero by the velocity V_F and yaw rate command that can be extracted from 6.10.

Hence, to apply the leader-follower formation keep based on virtual structure method suggested in [102] I propose the application of the control algorithm of a PID. The block diagram of the control scheme is shown in figure 6.7:
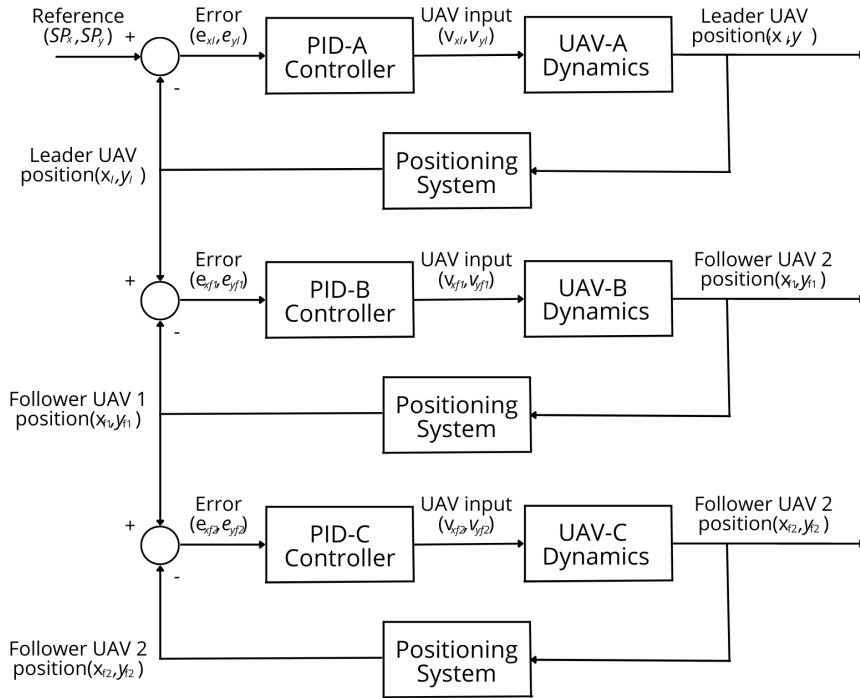
Figure 6.7: Block diagram of the leader–follower formation control loop proposed. *Source: own elaboration*

Nevertheless, due to some issues implementing the method that couldn't be redirected within the time given for the presentation of this bachelor's final thesis, it hasn't been possible to obtain graphical results.

The idea after the obtention of the corresponding results would have been the suggestion of a guidance system, implementing both the TFA and the leader-follower formation algorithms, to establish a method to optimize the area coverage of the swarm of UAVs.

Chapter 7

Multiplatform architecture

7.1 Communication

The UAVs can't directly transfer the flight data they collect to the Earth due to battery duration and the power required. Thus, the communication scheme suggested for this mission is shown in figure 7.1:
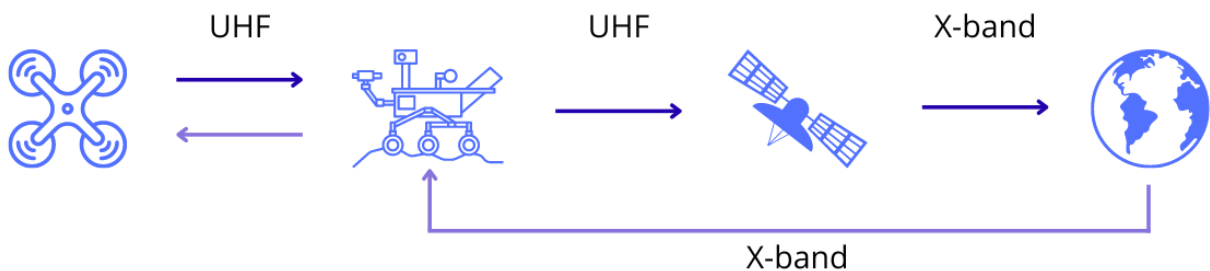
Figure 7.1: Communication scheme of the mission. *Source: own elaboration*

After the flight of the swarm, the UAV leader transfers the data collected to the rover leader through Ultra-High Frequency (UHF). Then, the rover sends the data to orbiter antennas through UHF (they are within close range of each other), whiches next transfer it to Earth operating in X-band. Finally, the data transference between Earth and the rover is done directly through X-band [20, 22, 40, 81, 103, 104].

7.1.1 The antennas

Deep Space Network (DSN)[105]:

The DSN is a worldwide telecommunications system operated by NASA's JPL that supports interplanetary spacecraft missions. It consists of three deep-space communication facilities spaced equidistant from each other at approximately 120° apart in longitude (see figure 7.2):

- The Goldstone Deep Space Communications Complex (in California, USA).

- The Madrid Deep Space Communications Complex (in Madrid, Spain).

- The Canberra Deep Space Communication Complex (in the southwest o Canberra, Australia).
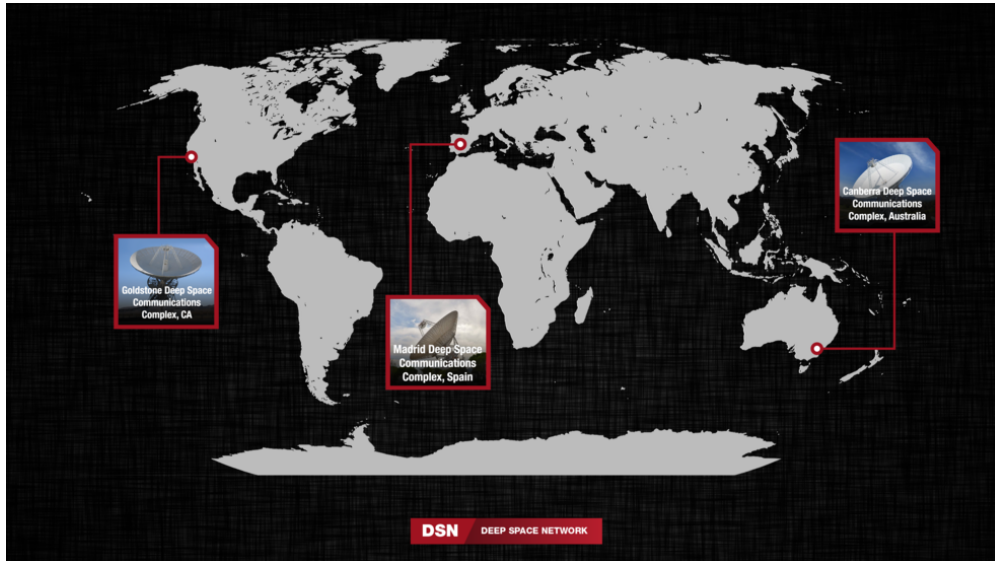
Figure 7.2: DSN Locations. *Source:* [106]

Its functions consist of:

- Acquiring, processing, decoding and distributing the scientifical data received.

- Sending commands to control the activities of spacecraft.

- Tracking communication between Earth and a spacecraft to allow flight controllers the determination of position and velocity with great precision.

- Performing science experiments using radio signals sent between Earth and a spacecraft.

- Performing its vital role as the communications hub for deep space exploration (it is used as an advanced instrument for radio astronomy and radar mapping of passing asteroids).

Mars Relay Network:

The Mars Relay Network [107, 108, 109] is a constellation of orbiters (see figure 7.3) involved in Mars Missions to ensure their continous and optimal development. Sending directly voluminous data from the rover to Earth takes a considerable amount of time, so most of it is sent through Mars orbiters, whiches provide highly efficient communications and reduce the duration taken.

The constelation is composed of the following spacecrafts:

- **Mars Reconnaissance Orbiter (MRO):** it is a NASA multi-mission spacecraft designed to study the climate and the geology of Mars, as well as investigating the potential hability of the planet for harbouring life. [110, 111]

- **Mars Atmospheric and Volatile EvolutioN (MAVEN)**: it is also a NASA spacecraft that studies the atmosphere and ionosphere of the red planet and how they interact with the Sun and solar wind [112, 113].

- **Mars Odyssey:** it is NASA's longest-lasting spacecraft at Mars. Its mission consists of investigating the Martian environment and providing significant information on crucial situations that future explorers shall face [114].

- **Mars Express:** it is ESA's first spacecraft to explore the red planet. Concretely, its primarly goals include the study of the atmosphere, climate, structure and geology of Mars, as well as searching for signs that indicate that the planet would have had water in the past [115].

- **ExoMars Trace Gas Orbiter (TGO):** it is a spacecraft of ESA, which primarly objective comprises the investigation of methane and other trace gases in the Martian atmosphere that might reveal signs of possible biological activity [116].

Figure 7.3: The Mars Relay Network. Clockwise from top left: NASA's Mars Reconnaissance Orbiter (MRO), Mars Atmospheric and Volatile EvolutioN (MAVEN), Mars Odyssey, and the European Space Agency's (ESA's) Mars Express and ExoMars Trace Gas Orbiter (TGO). *Source:* [117]

Table 7.1 illustrates the telecommunications characteristics of the orbiters that comprise the Mars Relay Network:

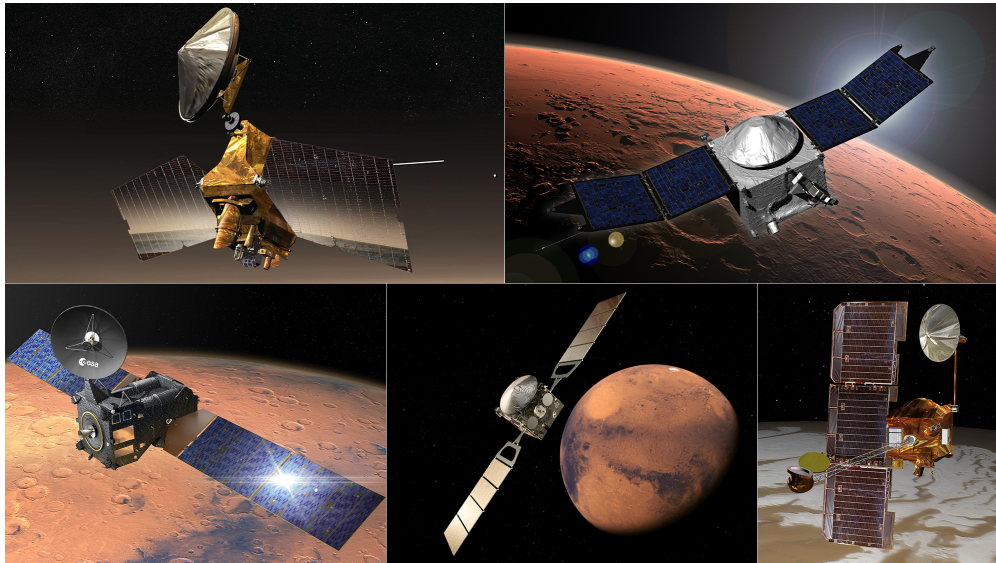|	Mars Reconnaissance Orbiter (MRO)	Mars Atmosphere and Volatile EvolutioN (MAVEN)	Mars Odyssey	Mars Express	ExoMars Trace Gas Orbiter (TGO)
Agency	NASA	NASA	NASA	ESA	ESA and Roscosmos
Launch	August 2005	November 2013	April 2001	June 2003	March 2016
Mars orbit insertion	March 2006	September 2014	October 2001	December 2003	October 2016
Orbit carachteristics	225 x 320 km, sun-synch	150 x 125 km sun-synch	400 x 400 sun-synch	250 x 10,142 km elliptical	200 x 98 km
UHF radio	Electra	Electra	CE-505	Melacom	Electra
Link protocol	CCSDS Proximity-1	CCSDS Proximity-1	CCSDS Proximity-1	CCSDS Proximity-1	CCSDS Proximity-1
Forward Link					
Frequency	435 - 450 MHz	435 - 450 MHz	437.1 MHz	437.1 MHz	390 - 450 MHz
Data rates	1,2,4,É, 1024 kbps	1,2,4,8, 2048 kbps	8 kbps	2,8 kbps	1, 2048 kbps
Coding	Uncoded or 7,1/2	7,1/2	Uncoded	Uncoded	Uncoded or 7,1/2
Return Link					
Frequency	390 - 405 MHz	390 - 405 MHz	401.6 MHz	401.6 MHz	390 - 450 MHz
Data rates	1,2,4,É, 1024 kbps	1,2,4,8, 2048 kbps	8,32,128,256 kbps	2,4,É, 128 kbps	1, 2048 kbps
Coding	(7,1/2) Convolutional	1024, 1/2	(7,1/2) Convolutional	(7,1/2) Convolutional	(7,1/2) Convolutional

Table 7.1: Comparison of telecommunications characteristics of the orbiters of the Mars Relay Network. *Source: own elaboration based on* [111, 118, 119]

7.1.2 Frequency bands

The frequency bands used in the suggested mission are the followings:

- **Ultra-High Frequency (UHF):** it is the International Telecommunications Union (ITU) designation for radio frequencies between 300 Mhz and 3 GHz. Their wavelenghts range from one meter to ten centimeters and they mainly propagate by line of sight (their waves travel in a direct path from the source to the receiver) [120, 121].

- **X-band:** this frequency is designated by the ITU as a satellite communications spectrum in the frequency range of 8 GHz to 12 GHz (Super High Frequency) for information exchange between space and Earth. Its characteristics are the followings [122, 123, 124]:

    - Minimal rain fade.

    - Resilience to interference.

    - High Power Spectral Density.

    - Flexible connectivity.

7.2 Connectivity

This section presents 2 End to End Information System (EEIS) architectures: the one used in 2016 and another one that only has been suggested in [125], but is expected to be applied in the future (between 2030 and 2040 approximately). Considering that the EEIS architecture used in 2016 is currently operating, the suggested mission would implement it. Nevertheless, this implementation does not exclude the proposed EEIS architecture for 2030-2040, which would offer better conditions.

7.2.1 2016 EEIS architecture (active)

The current EEIS architecture (see figure 7.4) is characterized by remote sensing, having a simple and reliable, but also constrained in many dimensions, connectivity on Mars. There are no cross-links between the orbiters and no data is exchanged between landed assets without returning the data to Earth.
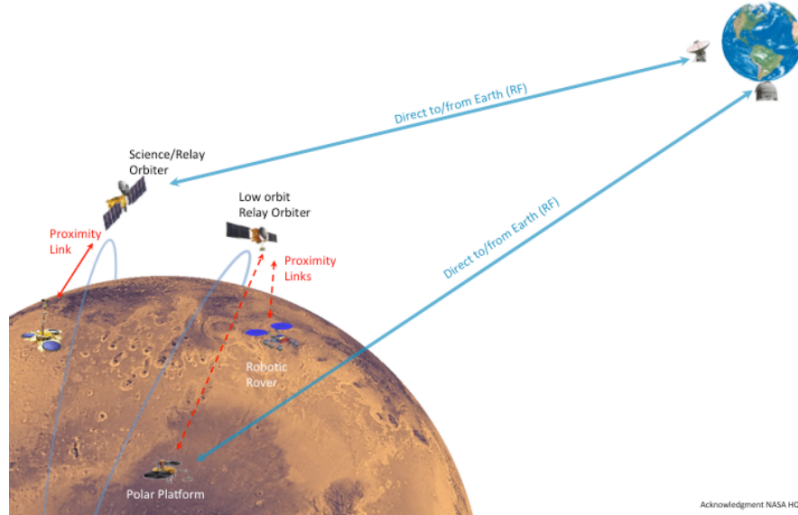
(a) Connectivity scheme of the Mars Relay Network. *Source:* [125]
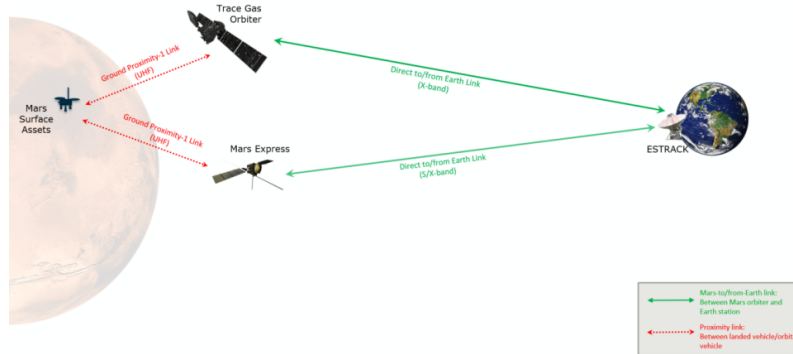
(b) Connectivity scheme of the ESA orbiters of the Mars Relay Network. *Source:* [126]

Figure 7.4: Connectivity schemes of the Mars Relay Network.

The current protocol view of the MRN for the E2E downlink path of the lander transfer frame is illustrated in figure 7.5:
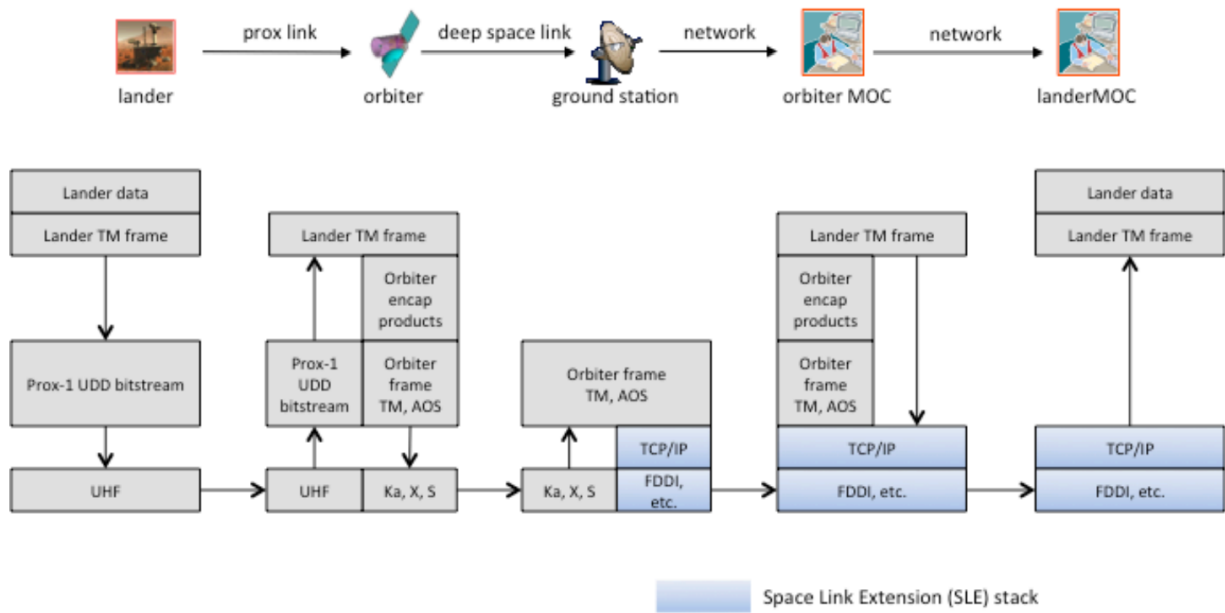
Figure 7.5: Protocol view scheme of the Mars Relay Network. *Source:* [125]

The diagram shows the different protocols that are used depending on the data system in the E2E data flow and where their begginnings and end points are.

7.2.2 Future EEIS architecture (suggestion)

In the near future, the surface of Mars will host more activities, so the suggested EEIS (see figure 7.6) not only will continue to include robotic remote sensing, but also other exploration assets. The concept of link directionality that is currently being used will disappear and communication pathways will be functionally symmetrical. This is due to the fact that the volume of required communication will need higher service levels, which will only be provided by satellites in aerostationary orbits.
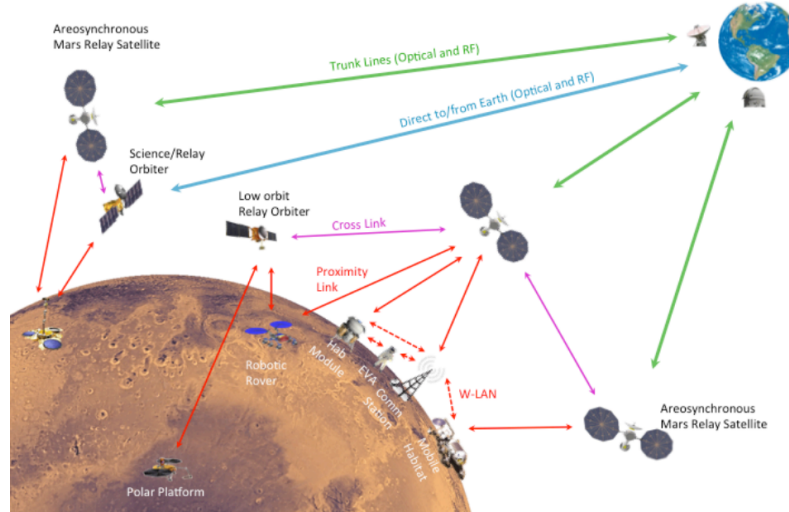
(a) Connectivity scheme suggested of the Mars Relay Network. *Source:* [125]
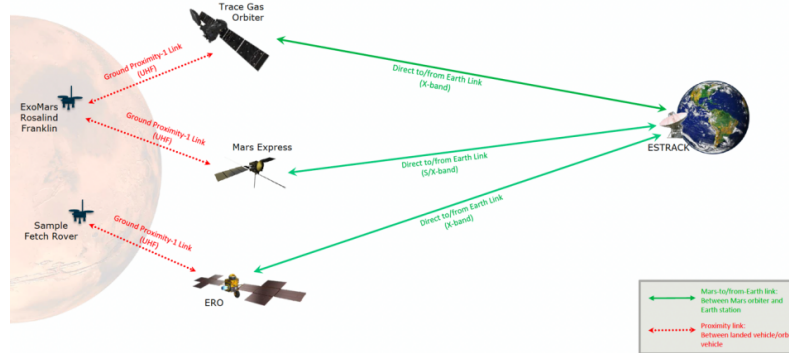
(b) Connectivity scheme suggested of the ESA orbiters of the Mars Relay Network. *Source:* [126]

Figure 7.6: Connectivity schemes suggested for the Mars Relay Network in future.

The suggested protocol view of the MRN is illustrated in figure 7.7:
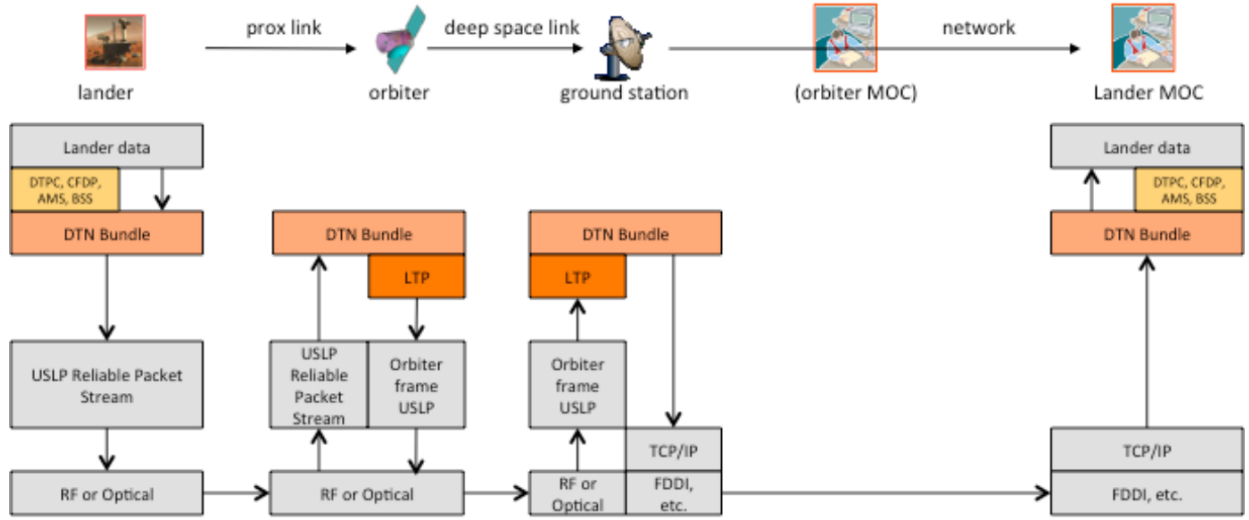
Figure 7.7: Protocol view scheme suggested of the Mars Relay Network. *Source:* [125]

The CCSDS Unified Space Data Link layer protocol (USLP) [127], which is compatible with a wide variety of coding and modulation schemes, is expected to be used.

Thus, the Mars Relay Network would provide a richer connectivity that would lead to alternative E2E paths that would be determined in terms of priority or destination by the Contact Graph Routing (CGR). In this way, when a mission operation team cancels or interrupts a planned communication, the Delay Tolerant Networking would automatically re-route it to the next most appropriate opportunity path.

Chapter 8

Budget summary

This section presents the budget summary (see table 8.1) of this bachelor's degree thesis, which has been estimated by calculating the technical cost redaction of the project. The itemized budget is illustrated in the budget document.

Area	Time (h)	Cost (€)
Research	250	3125
Report	205	2462.50
Computation	50	625
Power consumed	*considering the total time of 505 h*	9.31
Software licenses and material	-	1300
TOTAL	**505**	**7521.81**

Table 8.1: Budget summary. *Source: own elaboration.*

Chapter 9

Conclusions and future work

This final chapter is divided into 2 sections: conclusions and future work suggested.

9.1 Conclusions

The current bachelor's degree thesis presented three main goals:

1. Suggesting a mission located on Mars.

2. Making a preliminary study of a single UAV and its different subsystems.

3. Making a detailed study of the swarm formation.

In summary, at the end of this work, only two out of the three objectives have been achieved. Nevertheless, the technical viability of the proposed mission has been demonstrated.

Firstly, the available literature, research and technology make the proposal of a Martian mission, consisting on the cooperation of 2 swarms of UAVs and rovers and a constellation of orbiters possible. Furthermore, the mission architecture is also feasible and there are also different studies that propound improvements and upgrades in the field in the following years.

Secondly, it was presented a preliminary study of the overview of a single UAV and its different subsystems. The obtained satisfactory results were coherent with the available results of the Ingenuity helicopter and other studies.

Nevertheless, the third objective, which would have been a consistent part of this bachelor's degree thesis wasn't totally achieved. Although the Triangular Formation Algorithm was satisfactory implemented, the leader-follower formation keep algorithm wasn't appropriately applied due to different issues that couldn't be redirected within the time given for the presentation of this thesis. Because of this, the suggestion of a guidance system that implemented both the TFA and the leader-follower formation algorithms was not possible.

Moreover, it has to be noted that the most optimal method for the swarm formation of the UAVs would have been the implementation of a methaheuristic algorithm, based on artificial intelligence. However, it would have been necessary to extent the duration of this thesis to learn the essential concepts of this field and submit and implement the method. For this reason, it has been recommended as future work in the next section.

9.2 Future work

This bachelor's degree thesis is likely to be expanded at the following stages of the mission, introducing improvements in almost every aspect addressed. By topic, the improvement options in each chapter of the study are listed as follows:

- Studying in more detail the single UAV, going deeper into the different subsystems and moving up to the next levels of design.

  - Reviewing in detail the payload subsystem, studying the diverse instruments of the market to select or redesign the most appropriate option.

  - Studying in detail the Propulsion Subsystem, applying the Ducted Fan Design Code (DFDC) [128] and examining and choosing the most convenient aerodynamic profiles for the propellers.

  - Deeply studying the ADCS, selecting the most appropriate sensors in the market.

  - Regarding the Navigation Subsystem, analyzing the available instruments in the market and choosing and describing in detail the proper selection.

  - Making further research on the Power and Energy Subsystem, designing the electric diagram of the overall UAV.

  - Making a thermal investigation of the UAV to study the variation in the properties of the selected materials throughout the temperature.

  - Detailing the configuration of the landing gear and making a structural study of it.

  - Selecting the most appropriate model of antennas from the available in the market.

  - Regarding the Structural Subsystem, making a structural study of the overall UAV and designing a deployment mechanism to reduce the available area in the lander of the UAVs.

  - Designing the OBC Subsystem, suggesting machine learning algorithms.

- Drawing the CAD (Computer-Aided Design) of the overall UAV.

- Designing the flight control system of the UAV.

- Suggesting the approach of the overall mission from the beginning to the end.

- Redesign the lander of the UAVs to improve its capacity and performance.

- Suggesting an algorithm to process the images taken by the UAVS to chose the necessary ones and delete the rest to free up memory space.

- Designing in detail the parachutes of the UAVs and the landers of the swarms of UAVs and rovers.

- Studying in depth the swarm of rovers and the constellation of orbiters.

- Deeper researching the selected location for the mission by using the data from the Viking 1 and Mars Express orbiters.

- Implementing the leader-follower formation keep algorithm correctly.

- Suggesting a guidance system for the swarm of UAVs, implementing both the Triangular Formation and the leader-follower formation keep algorithms.

- Suggesting and implementing a metaheuristic algorithm based on path-based trajectories and swarm intelligence.

- Submiting and implementing an algorithm to detect caves that are likely to be viable sites for future Mars missions and future Martian bases.

References

1. UNIVERSITAT POLITÈCNICA DE CATALUNYA (UPC-ESEIAAT), Escola Superior d'Enginyeries Industrial Aeroespacial i Audiovisual de Terrassa. *REGLAMENT PER AL TREBALL DE FI DE GRAU (TFG) I TREBALL DE FI DE MASTER (TFM)*. 2018.

2. UNIVERSITAT POLITÈCNICA DE CATALUNYA (UPC-ESEIAAT), Escola Superior d'Enginyeries Industrial Aeroespacial i Audiovisual de Terrassa. PROCEDIMENT PER AL TREBALL DE FI D'ESTUDIS (TFE). 2018.

3. SHARMA, Manjula; GUPTA, Akshita; GUPTA, Sachin Kumar; ALSAMHI, Saeed Hamood; SHVETSOV, Alexey V. Survey on Unmanned Aerial Vehicle for Mars Exploration: Deployment Use Case. *Drones*. 2021, vol. 6, p. 4. ISSN 2504-446X. Available from DOI: `10.3390/drones6010004`.

4. MANNING, Rob (Engineer); SIMON, William L. *Mars rover Curiosity : an inside account from Curiosity's chief engineer*. [N.d.]. ISBN 9781588344731.

5. DRAKE, Bret G. *Human Exploration of Mars Design Reference Architecture 5.0 Mars Architecture Steering Group NASA Headquarters*. 2009. ISBN 3016210134. Available also from: `http://ston.jsc.nasa.gov/collections/TRS/`.

6. GRIP, Håvard F.; LAM, Johnny; BAYARD, David S.; CONWAY, Dylan T.; SINGH, Gurkirpal; BROCKERS, Roland; DELAUNE, Jeff H.; MATTHIES, Larry H.; MALPICA, Carlos; BROWN, Travis L.; JAIN, Abhinandan; MARTIN, Alejandro M. San; MEREWETHER, Gene B. Flight Control System for NASA's Mars Helicopter. In: American Institute of Aeronautics and Astronautics, 2019. ISBN 978-1-62410-578-4. Available from DOI: `10.2514/6.2019-1289`.

7. SAND, S.; ZHANG, S.; MUHLEGG, M.; FALCONI, G.; ZHU, C.; KRUGER, T.; NOWAK, S. Swarm exploration and navigation on mars. In: IEEE, 2013, pp. 1–6. ISBN 978-1-4799-0486-0. Available from DOI: `10.1109/ICL-GNSS.2013.6577272`.

8. PROGRAM, Mars Exploration; NASA'S SCIENCE MISSION DIRECTORATE, Jet Propulsion Laboratory for. *Mars Exploration Program*. Available also from: `https://mars.nasa.gov/`. [Accessed: October 6, 2022].

9. *Viking Lander Model*. 2007. Available also from: `https://www.jpl.nasa.gov/images/pia09703-viking-lander-model`. [Accessed: October 6, 2022].

10. *Mars Exploration Rovers Overview*. Available also from: `https://mars.nasa.gov/mer/mission/overview/`. [Accessed: October 6, 2022].

11. *Curiosity's Selfie at Mont Mercou.* Available also from: `https://mars.nasa.gov/resources/25757/curiositys-selfie-at-mont-mercou/?site=msl`. [Accessed: October 6, 2022].

12. *Perseverance's Selfie at "Rochette".* Available also from: `https://mars.nasa.gov/resources/26253/perseverances-selfie-at-rochette/`. [Accessed: October 6, 2022].

13. *Ingenuity Deployed on Mars.* Available also from: `https://mars.nasa.gov/resources/25781/ingenuity-deployed-on-mars/`. [Accessed: October 6, 2022].

14. *InSight's First Selfie.* Available also from: `https://mars.nasa.gov/resources/22211/insights-first-selfie/?site=insight`. [Accessed: October 6, 2022].

15. HARBAUGH, Jennifer; DUNBAR, Brian. *Discovery Program.* 2022. Available also from: `https://www.nasa.gov/planetarymissions/discovery.html`. [Accessed: October 6, 2022].

16. DINO, Jonas; DUNBAR, Brian. *Phoenix Mars Scout (includes NASA Ames partnership).* 2008. Available also from: `https://www.nasa.gov/centers/ames/missions/2007/phoenix.html`. [Accessed: October 6, 2022].

17. *ExoMars Rover and Surface Platform (ESA).* 2022. Available also from: `https://mars.nasa.gov/mars-exploration/missions/esa-exomars-rover/`. [Accessed: October 6, 2022].

18. FANTINO, E.; GRASSI, M.; PASOLINI, P.; CAUSA, F.; MOLFESE, C.; AURIGEMMA, R.; CIMMINIELLO, N.; TORRE, D. de la; DELL'AVERSANA, P.; ESPOSITO, F.; GRAMICCIA, L.; PAUDICE, F.; PUNZO, F.; ROMA, I.; SAVINO, R.; ZUPPARDI, G. The Small Mars System. *Acta Astronautica.* 2017, vol. 137, pp. 168–181. ISSN 00945765. Available from DOI: `10.1016/j.actaastro.2017.04.024`. Paper 28.

19. HARBAUGH, Jennifer; DUNBAR, Brian. *New Frontiers Program.* Available also from: `https://www.nasa.gov/planetarymissions/newfrontiers.html`. [Accessed: October 6, 2022].

20. JPL-CALTECH, NASA/. Ingenuity Landing Press Kit. [N.d.].

21. *Mars 2020 Mission.* Available also from: `https://mars.nasa.gov/mars2020/`. [Accessed: October 6, 2022].

22. BALARAM, J.; AUNG, Mi Mi; GOLOMBEK, Matthew P. *The Ingenuity Helicopter on the Perseverance Rover.* Springer Science and Business Media B.V., 2021-06. ISSN 15729672.

23. LORENZ, Ralph D; TURTLE, Elizabeth P; BARNES, Jason W; TRAINER, Melissa G; ADAMS, Douglas S; HIBBARD, Kenneth E; SHELDON, Colin Z; ZACNY, Kris; PEPLOWSKI, Patrick N; LAWRENCE, David J; RAVINE, Michael A; MCGEE, Timothy G; SOTZEN, Kristin S; MACKENZIE, Shannon M; LANGELAAN, Jack W; SCHMITZ, Sven; WOLFARTH, Lawrence S; BEDINI, Peter D. *Dragonfly: A Rotorcraft Lander Concept for Scientific Exploration at Titan FORMULATION OF THE DRAGONFLY CONCEPT.* 2018. Available also from: `www.jhuapl.edu/techdigest`.

24. MCGEE, Timothy G.; ADAMS, Douglas; HIBBARD, Kenneth; TURTLE, Elizabeth; LORENZ, Ralph; AMZAJERDIAN, Farzin; LANGELAAN, Jacob. Guidance, Navigation, and Control for Exploration of Titan with the Dragonfly Rotorcraft Lander. In: *2018 AIAA Guidance, Navigation, and Control Conference.* [N.d.]. Available from DOI: `10.2514/6.2018-1330`.

25. GRIP, Håvard Fjær; SCHARF, Daniel P.; MALPICA, Carlos; JOHNSON, Wayne; MANDIĆ, Milan; SINGH, Gurkirpal; YOUNG, Larry. Guidance and control for a mars helicopter. In: American Institute

of Aeronautics and Astronautics Inc, AIAA, 2018, vol. 0. ISBN 9781624105265. Available from DOI: `10.2514/6.2018-1849`. Paper 5.

26. NEJJARI, Fatiha. *UAV Guidance and Autonomous Control Module 1: UAV Modelling and Simulation.* UPC lectures.

27. *RoboSeed Nano.* Available also from: `https://en.wikipedia.org/wiki/RoboSeed_Nano`. [Accessed: October 12, 2022].

28. *Stella X8 Multirotor Frame Patent-holding.* Available also from: `https://hdairstudio.com/product/stella-x8-multirotor/`. [Accessed: October 12, 2022].

29. AKYURT, Engin. *Quadrotor.* Available also from: `https://pixabay.com/photos/drone-camera-drone-quadcopter-5578998/`. [Accessed: October 12, 2022].

30. *Global Multi Rotor Drone Market Research Report: Ken Research.* 2020-02. Available also from: `https://www.kenresearch.com/blog/2020/02/global-multi-rotor-drone-market/`. [Accessed: October 12, 2022].

31. BOUABDALLAH, Samir. Design and Control of quadrotors with application to autonomous flying. 2007. Available from DOI: `10.5075/epfl-thesis-3727`.

32. DATTA, Anubhav; ROGET, Beatrice; GRIFFITHS, Daniel; PUGLIESE, Gregory; SITARAMAN, Jayanarayanan; BAO, Jinsong; LIU, Lin; GAMARD, Olivier. Design of a Martian autonomous rotary-wing vehicle. *Journal of Aircraft.* 2003, vol. 40, pp. 461–472. ISSN 15333868. Available from DOI: `10.2514/2.3141`.

33. PATEL, Akash. *Design, Modelling and Control of a Space UAV for Mars Exploration.* 2021.

34. STAFF, IEEE; STAFF, IEEE. *2011 8th International Conference on Ubiquitous Robots and Ambient Intelligence.* [N.d.]. ISBN 9781457707230.

35. *Mars Fact Sheet.* Available also from: `https://nssdc.gsfc.nasa.gov/planetary/factsheet/marsfact.html`. [Accessed: October 17, 2022].

36. COLOZZA, Anthony. *Airships for Planetary Exploration.* ISBN 2004213345. Available also from: `http://www.sti.nasa.gov`.

37. FISHBAUGH, Kathryn E; HEAD, James W. Comparison of the North and South Polar Caps of Mars: New Observations from MOLA Data and Discussion of Some Outstanding Questions. *Icarus.* 2001, vol. 154, no. 1, pp. 145–161. ISSN 0019-1035. Available from DOI: `https://doi.org/10.1006/icar.2001.6666`.

38. MCGOWAN, Eileen. Spatial distribution of putative water related features in Southern Acidalia/Cydonia Mensae, Mars. *Icarus.* 2009, vol. 202, no. 1, pp. 78–89. ISSN 0019-1035. Available from DOI: `https://doi.org/10.1016/j.icarus.2009.02.024`.

39. SUREDA, Miquel. *Spacecraft Design.* 2020. UPC lectures.

40. PERGOLA, Pierpaolo; CIPOLLA, Vittorio. Mission architecture for Mars exploration based on small satellites and planetary drones. *International Journal of Intelligent Unmanned Systems.* 2016, vol. 4, pp. 142–162. ISSN 20496435. Available from DOI: `10.1108/IJIUS-12-2015-0014`.

41. PARKER, Timothy J; SCHNEEBERGER, Dale M; PIERI, David C; SAUNDERS, R Stephen. *Curvilinear Ridges and related features in southwest Cydonia Mensae. Mars.*

42. Atlas of Mars: Quadrangles MTM 40007, 40012, 40017, 45007, 45012, AND 45017. [N.d.].

43. GUEST, J. E.; BUTTERWORTH, P. S.; GREELEY, R. Geological observations in the Cydonia Region of Mars from Viking. *Journal of Geophysical Research*. 1977, vol. 82, pp. 4111–4120. Available from DOI: `10.1029/js082i028p04111`.

44. *Mars Atlas*. Available also from: `https://mars.nasa.gov/gallery/atlas/index.html`. [Accessed: October 13, 2022].

45. TRUSZKOWSKI, Walt; HALLOCK, Harold L.; ROUFF, Christopher; KARLIN, Jay; RASH, James; HINCHEY, Mike; STERRITT, Roy. *NASA Monographs in Systems and Software Engineering*.

46. RAHMANI, Amir; BANDYOPADHYAY, Saptarshi; ROSSI, Federico; CROIX, Jean-Pierre De La; HOOK, Joshua Vander; WOLF, Michael. *Space Vehicle Swarm Exploration Missions: A Study of Key Enabling Technologies and Gaps*.

47. CHICARRO, Augustin; MARTIN, Patrick; TRAUTNER, R. The Mars Express mission: an overview. *Mars Express: the scientific payload*. 2004, vol. 1240, pp. 3–13.

48. *The spacecraft*. Available also from: `https://www.esa.int/Science_Exploration/Space_Science/Mars_Express/The_spacecraft`. [Accessed: November 6, 2022].

49. EDQUIST, Karl T.; HOLLIS, Brian R.; DYAKONOV, Artem A.; LAUB, Bernard; WRIGHT, Michael J.; RIVELLINI, Tomasso P.; SLIMKO, Eric M.; WILLCOCKSON, William H. Mars science laboratory entry capsule aerothermodynamics and thermal protection system. In: 2007. ISBN 1424405254. ISSN 1095323X. Available from DOI: `10.1109/AERO.2007.352823`.

50. EDQUIST, Karl T; DYAKONOV, Artem A; WRIGHT, Michael J; TANG, Chun Y. *Aerothermodynamic Design of the Mars Science Laboratory Heatshield*.

51. CHEN, David W Way Richard W Powell Allen; STELTZNER, Adam D; MARTIN, A Miguel San; BURKHART, P Daniel; MENDECK, Gavin F. *Mars Science Laboratory: Entry, Descent, and Landing System Performance*.

52. JPL. *Mars Curiosity Rover*. Available also from: `https://mars.nasa.gov/msl/spacecraft/getting-to-mars/`. [Accessed: November 26, 2022].

53. NASA/JPL-CALTECH. *Mars Science Laboratory Aeroshell with Curiosity Inside*. Available also from: `https://mars.nasa.gov/resources/3667/mars-science-laboratory-aeroshell-with-curiosity-inside/`. [Accessed: November 26, 2022].

54. NASA/JPL-CALTECH. *Entry, Descent, and Landing*. Available also from: `https://mars.nasa.gov/mars2020/timeline/landing/entry-descent-landing/`. [Accessed: December 27, 2022].

55. NASA/JPL-CALTECH. *Perseverance Rover's Entry, Descent and Landing Profile*. Available also from: `https://mars.nasa.gov/resources/25489/perseverance-rovers-entry-descent-and-landing-profile/`. [Accessed: December 27, 2022].

56. *Perseverance's Selfie at "Rochette"*. Available also from: `https://mars.nasa.gov/resources/26253/perseverances-selfie-at-rochette/`. [Accessed: November 6, 2022].

57. *Mars 2020 Mission Overview*. Available also from: `https://mars.nasa.gov/mars2020/mission/overview/`. [Accessed: November 6, 2022].

58. *Instruments.* Available also from: `https://mars.nasa.gov/mars2020/spacecraft/instruments/`. [Accessed: November 6, 2022].

59. WILLIFORD, Kenneth H.; FARLEY, Kenneth A.; STACK, Kathryn M.; ALLWOOD, Abigail C.; BEATY, David; BEEGLE, Luther W.; BHARTIA, Rohit; BROWN, Adrian J.; DE LA TORRE JUAREZ, Manuel; HAMRAN, Svein-Erik; HECHT, Michael H.; HUROWITZ, Joel A.; RODRIGUEZ-MANFREDI, Jose A.; MAURICE, Sylvestre; MILKOVICH, Sarah; WIENS, Roger C. Chapter 11 - The NASA Mars 2020 Rover Mission and the Search for Extraterrestrial Life. In: CABROL, Nathalie A.; GRIN, Edmond A. (eds.). *From Habitability to Life on Mars.* Elsevier, 2018, pp. 275–308. ISBN 978-0-12-809935-3. Available from DOI: `https://doi.org/10.1016/B978-0-12-809935-3.00010-4`.

60. REKLEITIS, Ioannis; BEDWANI, Jean-Luc; DUPUIS, Erick. Autonomous planetary exploration using LIDAR data. In: *2009 IEEE International Conference on Robotics and Automation.* 2009, pp. 3025–3030. Available from DOI: `10.1109/ROBOT.2009.5152504`.

61. GUSMÃO, Guilherme; BARBOSA, C.; RAPOSO, Alberto. Development and Validation of LiDAR Sensor Simulators Based on Parallel Raycasting. *Sensors.* 2020, vol. 20, p. 7186. Available from DOI: `10.3390/s20247186`.

62. PHILLIPS, Robin; PALLADINO, Massimo; COURTOIS, Camille. Development of brushed and brushless DC motors for use in the ExoMars drilling and sampling mechanism. In: *Proceedings of the 41st Aerospace Mechanisms Symposium.* 2012, pp. 16–18.

63. DEKAN, Martin; DUCHOŇ, F; JURIŠICA, L; VITKO, A. Probabilistic model of laser rangefinder. *AD ALTA: Journal of Interdisciplinary Research.* 2011, vol. 1, no. 2, pp. 151–155.

64. WITHROW-MASER, Shannah; JOHNSON, Wayne; YOUNG, Larry; KONING, Witold; KUANG, Winnie; MALPICA, Carlos; BALARAM, J; TZANETOS, Theodore. *Mars Science Helicopter: Conceptual Design of the Next Generation of Mars Rotorcraft.*

65. BALARAM, J. Bob; CANHAM, Timothy; DUNCAN, Courtney; GOLOMBEK, Matt; GRIP, Håvard Fjær; JOHNSON, Wayne; MAKI, Justin; QUON, Amelia; STERN, Ryan; ZHU, David. Mars helicopter technology demonstrator. In: American Institute of Aeronautics and Astronautics Inc, AIAA, 2018. ISBN 9781624105258. Available from DOI: `10.2514/6.2018-0023`.

66. BORTHOMIEU, Y.; SEMERIE, J. -P. SAFT VES180 SA High Specific Energy Cell Qualification. In: WILSON, A. (ed.). *ESA Special Publication.* 2005, vol. 589, p. 58. ESA Special Publication.

67. APPELBAUM, Joseph; FLOOD, Dennis J. Solar radiation on Mars. *Solar Energy.* 1990, vol. 45, pp. 353–363. ISSN 0038092X. Available from DOI: `10.1016/0038-092X(90)90156-7`.

68. NASA/JPL-CALTECH. *Mars Perseverance Sol 46: WATSON Camera.* 2021. Available also from: `https://mars.nasa.gov/mars2020/multimedia/raw-images/SI1_0046_0671022109_238ECM_N0031416SRLC07021_000085J`. [Accessed: December 21, 2022].

69. LI, J.; AIERKEN, A.; LIU, Y.; ZHUANG, Y.; YANG, X.; MO, J. H.; FAN, R. K.; CHEN, Q. Y.; ZHANG, S. Y.; HUANG, Y. M.; ZHANG, Q. *A Brief Review of High Efficiency III-V Solar Cells for Space Application.* Vol. 8. Frontiers Media S.A., 2021. ISSN 2296424X. Available from DOI: `10.3389/fphy.2020.631925`.

70. ELECTRICAL, Institute of; ENGINEERS, Electronics. *2017 IEEE 44th Photovoltaic Specialist Conference (PVSC) : 25-30 June 2017*. [N.d.]. ISBN 9781509056057.

71. RAFFAMAIDEN. *A p–n junction*. Available also from: `https://n9.cl/eor0q`. [Accessed: December 21, 2022].

72. SCHMIDT, Tyler M; CAPPUCCI, Stefano; MILLER, Jennifer R; WAGNER, Mark F; BHANDARI, Pradeep; PAUKEN, Michael T. *Thermal Design of a Mars Helicopter Technology Demonstration Concept*. 2018.

73. PIPENBERG, Benjamin T.; KEENNON, Matthew T.; TYLER, Jeremy D.; LANGBERG, Sara A.; HIBBS, Bart; BALARAM, J. (Bob); GRIP, Håvard F.; PEMPEJIAN, Jack. Design and fabrication of the mars helicopter rotor, airframe, and landing gear systems. In: American Institute of Aeronautics and Astronautics Inc, AIAA, 2019. ISBN 9781624105784. Available from DOI: `10.2514/6.2019-0620`.

74. *Designing Dragonfly, NASA's Titan explorer*. 2022-10. Available also from: `https://aerospaceamerica.aiaa.org/features/designing-dragonfly-nasas-titan-explorer/`. [Accessed: November 26, 2022].

75. WITHROW-MASER, Shannah; JOHNSON, Wayne; YOUNG, Larry; KONING, Witold; KUANG, Winnie; MALPICA, Carlos; BALARAM, J; TZANETOS, Theodore. *Mars Science Helicopter: Conceptual Design of the Next Generation of Mars Rotorcraft*.

76. *6,0m² (69J 8kg Multirotor) - Opale drone rescue parachute*. Available also from: `https://parachutedrone.com/en/home/8-opale-drone-rescue-parachute-6m2-69j-8kg-multirotor.html?search_query=Opale+drone+rescue+parachute&results=51`. [Accessed: November 26, 2022].

77. CRUZ, Juan R. *Parachutes for Planetary Entry Systems*.

78. EWING, E. G.; BIXBY, H. W.; KNACKE, T. W. Recovery Systemps Design Guide. 1975.

79. *Technology by the Zigbee Alliance enables communication on Mars*. Available also from: `https://www.develcoproducts.com/blog/technology-by-the-zigbee-alliance-enables-communication-on-mars/`. [Accessed: November 17, 2022].

80. *ZigBeeProtocol*. 2015-08.

81. RENNES 1, Université de. *On Mars, the amazing design of the radio link between Ingenuity and the Perseverance rover*. YouTube, [n.d.]. Available also from: `https://youtu.be/GzteogKj5d8`.

82. *Satellite frequency bands*. Available also from: `https://www.esa.int/Applications/Telecommunications_Integrated_Applications/Satellite_frequency_bands`. [Accessed: November 17, 2022].

83. *Composites TeXtreme materials go to Mars*. 2021. Available also from: `https://www.innovationintextiles.com/textreme-materials-go-to-mars/`.

84. *The Mars Helicopter - Ingenuity*. 2021-12. Available also from: `https://www.textreme.com/the-mars-helicopter-ingenuity/`. [Accessed: November 26, 2022].

85. *Onboard Computers*. Available also from: `https://www.esa.int/Enabling_Support/Space_Engineering_Technology/Onboard_Computers_and_Data_Handling/Onboard_Computers`. [Accessed: November 26, 2022].

86. *F' Flight Software Embedded Systems Framework*. Available also from: `https://nasa.github.io/fprime/`. [Accessed: November 26, 2022].

87. *Meet the Open-Source Software Powering NASA's Ingenuity Mars Helicopter.* Available also from: `https://www.jpl.nasa.gov/news/meet-the-open-source-software-powering-nasas-ingenuity-mars-helicopter`. [Accessed: November 26, 2022].

88. *ISS-RapidScat.* Available also from: `https://www.jpl.nasa.gov/missions/international-space-station-rapid-scatterometer-iss-rapidscat`. [Accessed: November 26, 2022].

89. *Tiny Satellite for Studying Distant Planets Goes Quiet.* Available also from: `https://www.jpl.nasa.gov/news/tiny-satellite-for-studying-distant-planets-goes-quiet`. [Accessed: November 26, 2022].

90. BAILLIEUL, J.; SURI, A. Information patterns and Hedging Brockett's theorem in controlling vehicle formations. In: *42nd IEEE International Conference on Decision and Control (IEEE Cat. No.03CH37475).* 2003, vol. 1, 556–563 Vol.1. Available from DOI: `10.1109/CDC.2003.1272622`.

91. LEONARD, Naomi Ehrich; PALEY, Derek A.; LEKIEN, Francois; SEPULCHRE, Rodolphe; FRATAN-TONI, David M.; DAVIS, Russ E. Collective Motion, Sensor Networks, and Ocean Sampling. *Proceedings of the IEEE.* 2007, vol. 95, no. 1, pp. 48–74. Available from DOI: `10.1109/JPROC.2006.887295`.

92. WANG, Qin; HUA, Qingguang; CHEN, Zuwen. Globally exponentially stable triangle formation control of multi-robot systems. In: Springer Verlag, 2016, vol. 405, pp. 361–370. ISBN 9789811023347. ISSN 18761119. Available from DOI: `10.1007/978-981-10-2335-4_34`.

93. CAO, M; MORSE, A S; YU, C; ANDERSON, B D O; DASGUPTA, S. *Controlling a Triangular Formation of Mobile Autonomous Agents.*

94. NEUKUM), ESA/DLR/FU Berlin (G. *'Pyramids and Skull' in Cydonia region, perspective.* 2006. Available also from: `https://www.esa.int/ESA_Multimedia/Images/2006/09/Pyramids_and_Skull_in_Cydonia_region_perspective#.Y7SxhGKXEQO.link`. [Accessed: December 26, 2022].

95. ARDUINO. *Language Reference.* Available also from: `https://www.arduino.cc/reference/en/`. [Accessed: December 27, 2022].

96. SENSORTECH, Bosh. *BMI160. Small, low power intertial measurement unit.* 2020.

97. OY, Murata Electronics. *The SCA100T Dual Axis Inclinometer Series.* [N.d.]. Available also from: `www.muratamems.fi`.

98. GARMIN. *Lidar Lite v3 Operation Manual and Technical Specifications.* 2016.

99. BASSOLILLO, Salvatore Rosario; BLASI, Luciano; D'AMATO, Egidio; MATTEI, Massimiliano; NOTARO, Immacolata. Decentralized Triangular Guidance Algorithms for Formations of UAVs. *Drones.* 2022, vol. 6. ISSN 2504446X. Available from DOI: `10.3390/drones6010007`.

100. GOOS, Gerhard; HARTMANIS, Juris; VAN, Jan; BOARD, Leeuwen Editorial; HUTCHISON, David; KANADE, Takeo; KITTLER, Josef; KLEINBERG, Jon M; KOBSA, Alfred; MATTERN, Friedemann; ZURICH, Eth; MITCHELL, John C; NAOR, Moni; NIERSTRASZ, Oscar; STEFFEN, Bernhard; SUDAN, Madhu; TERZOPOULOS, Demetri; TYGAR, Doug; WEIKUM, Gerhard. *LNCS 5592 - Computational Science and Its Applications - ICCSA 2009.* 2009.

101. CAO, Ming; YU, Changbin; ANDERSON, Brian D.O. Formation control using range-only measurements. *Automatica.* 2011, vol. 47, pp. 776–781. ISSN 00051098. Available from DOI: `10.1016/j.automatica.2011.01.067`.

102. EDWARDS, D.B.; BEAN, T.A.; ODELL, D.L.; ANDERSON, M.J. A leader-follower algorithm for multiple AUV formations. In: *2004 IEEE/OES Autonomous Underwater Vehicles (IEEE Cat. No.04CH37578)*. 2004, pp. 40–46. Available from DOI: `10.1109/AUV.2004.1431191`.

103. NASA. *Communications*. Available also from: `https://mars.nasa.gov/mars2020/spacecraft/rover/communications/`. [Accessed: November 19, 2022].

104. JPL. *Telecommunications: How Perseverance Talks to Earth*. Available also from: `https://www.jpl.nasa.gov/news/press_kits/mars_2020/landing/mission/spacecraft/telecommunications/`. [Accessed: November 19, 2022].

105. NASA. *What is the Deep Space Network?* 2020. Available also from: `https://www.nasa.gov/directorates/heo/scan/services/networks/deep_space_network/about`. [Accessed: November 20, 2022].

106. NASA. *DSN Complexes*. 2022-02. Available also from: `https://www.nasa.gov/directorates/heo/scan/services/networks/deep_space_network/complexes`. [Accessed: November 19, 2022].

107. JPL. *The Mars Relay Network Connects Us to NASA's Martian Explorers*. Available also from: `https://mars.nasa.gov/news/8861/the-mars-relay-network-connects-us-to-nasas-martian-explorers/`. [Accessed: November 20, 2022].

108. NASA. *Mars Relay Network*. Available also from: `https://eyes.nasa.gov/apps/mrn/#/mars`. [Accessed: November 20, 2022].

109. EDWARDS, C.D.; ARNOLD, B.; DEPAULA, R.; KAZZ, G.; LEE, Charles; NOREEN, G. Relay communications strategies for Mars exploration through 2020. *Acta Astronautica*. 2006, vol. 59, pp. 310–318. Available from DOI: `10.1016/j.actaastro.2006.02.038`.

110. NASA. *Mars Reconnaissance Orbiter*. 2021-02. Available also from: `https://solarsystem.nasa.gov/missions/mars-reconnaissance-orbiter/in-depth/`. [Accessed: November 26, 2022].

111. NASA. *Mars Reconnaissance Orbiter*. 2022-05. Available also from: `https://n9.cl/zgzr9`. [Accessed: December 27, 2022].

112. NASA. *MAVEN*. 2021-02. Available also from: `https://solarsystem.nasa.gov/missions/maven/in-depth/`. [Accessed: November 26, 2022].

113. CHAMBERLAIN, Neil; GLADDEN, Roy; BRUVOLD, Kris. MAVEN relay operations concept. In: *2012 IEEE Aerospace Conference*. 2012, pp. 1–11. Available from DOI: `10.1109/AERO.2012.6187114`.

114. NASA. *Mars Odyssey*. 2021-02. Available also from: `https://solarsystem.nasa.gov/missions/mars-odyssey/in-depth/`. [Accessed: November 26, 2022].

115. NASA. *Mars Express*. 2018-11. Available also from: `https://solarsystem.nasa.gov/missions/mars-express/in-depth/`. [Accessed: November 26, 2022].

116. NASA. *ExoMars Trace Gas Orbiter / Schiaparelli*. 2019-04. Available also from: `https://solarsystem.nasa.gov/missions/exomars-trace-gas-orbiter-schiaparelli/in-depth/`. [Accessed: November 26, 2022].

117. NASA. *Five Spacecraft of the Mars Relay Network*. Available also from: `https://mars.nasa.gov/resources/25589/five-spacecraft-of-the-mars-relay-network/`. [Accessed: November 20, 2022].

118. EDWARDS, JR., C.D.; ARNOLD, B.; DEPAULA, R.; KAZZ, G.; LEE, C.; NOREEN, G. Relay communications strategies for Mars exploration through 2020. *Acta Astronautica*. 2006, vol. 59, no. 1, pp. 310–318. ISSN 0094-5765. Available from DOI: `https://doi.org/10.1016/j.actaastro.2006.02.038`. Space for Inspiration of Humankind, Selected Proceedings of the 56th International Astronautical Federation Congress, Fukuoka, Japan, 17-21 October 2005.

119. ESA. *ExoMars/TGO operations*. Available also from: `https://www.esa.int/Enabling_Support/Operations/ExoMars_TGO_operations`. [Accessed: December 27, 2022].

120. CORPORATION, Alliance. *What is the UHF Frequency Band?* 2018-10. Available also from: `https://alliancecorporation.ca/news/vendor-news-announcements/what-is-the-uhf-frequency-band/`. [Accessed: November 26, 2022].

121. NASA. *Communications*. Available also from: `https://mars.nasa.gov/mars2020/spacecraft/rover/communications/#UHF-Antenna`. [Accessed: November 26, 2022].

122. NASA. *X-band Communications*. Available also from: `https://mars.nasa.gov/mro/mission/communications/commxband/`. [Accessed: November 26, 2022].

123. *Comunicación satelital de banda X*. Available also from: `https://hmong.es/wiki/X_Band_Satellite_Communication`. [Accessed: November 26, 2022].

124. ESA. *Satellite frequency bands*. Available also from: `https://www.esa.int/Applications/Telecommunications_Integrated_Applications/Satellite_frequency_bands`. [Accessed: November 26, 2022].

125. KAZZ, Greg J.; BURLEIGH, Scott; CHEUNG, Kar Ming; SHAH, Biren. Evolution of the Mars relay network end-to-end information system in the Mars human era (2030-2040). In: American Institute of Aeronautics and Astronautics Inc, AIAA, 2016. ISBN 9781624104268. Available from DOI: `10.2514/6.2016-2420`.

126. NASA, Co-chairs Wallace Tai Marco Lanucara; ESA, JPL; KOGA, Gan A Yong CNSA Peng Jing CNSA Nicola Maturo ESA R Srinivas ISRO Hirokazu Hoshino JAXA Masaru; NASA, David Israel; COSBY, GSFC Matthew. *Mars and Beyond Communications Architecture Working Group-Membership Change Log*.

127. CCSDS; NASA. *Recommendation for Space Data System Standards UNIFIED SPACE DATA LINK PROTOCOL RECOMMENDED STANDARD CCSDS 732.1-B-2 BLUE BOOK*. 2021.

128. YOUNGREN, Harold; DRELA, Mark; SANDERS, Scott. *Ducted Fan Design Code (DFDC)*. 2005-12. Available also from: `https://web.mit.edu/drela/Public/web/dfdc/`. [Accessed: October 10, 2022].